environments

MDPI

Review

Progress in Graphene Oxide Hybrids for Environmental Applications

Edith Flora Joel * and Galina Lujanienė

SRI Center for Physical Sciences and Technology, Savanorių av. 231, LT-02300 Vilnius, Lithuania
* Correspondence: edith.joel@ftmc.lt

Abstract: Graphene-oxide-based metal hybrids (GM) are used for the rapid and efficient reduction and removal of toxic adulterants in the environment. The exceptionally high specific surface area, versatile surface chemistry, and exceptional customization efficiency of graphene oxide nanosheets combined with the adaptable chemistry of metal nanoparticles enable the formation of GM hybrid nanocomposites. However, little is known about the architecture of GM nanocomposite engineering, interaction mechanisms, and environmental compatibility. This review aims to describe the environmental performance of graphene oxide–metal hybrids for the removal of environmental pollutants, carbon capture, EMI shielding efficiency, and microbial elimination of engineered graphene oxide composites anchored with metal particles. We also developed an essential link between the material properties of GM nanohybrids and their performance, which identified the fundamental parameters that influence the contaminant removal capability and EMI resistance efficiency. The influence of the thermodynamic parameters of GM on the adsorption of radioisotopes, heavy metals, organic pollutants, and dyes was considered. Finally, we comment on the remaining challenges and provide suggestions for future developments in this field.

Keywords: graphene oxide; metallic nanoparticles; gas capture; water purification; antibacterial

Citation: Joel, E.F.; Lujanienė, G. Progress in Graphene Oxide Hybrids for Environmental Applications. *Environments* **2022**, *9*, 153. https://doi.org/10.3390/environments9120153

Academic Editor: Dino Musmarra

Received: 12 October 2022
Accepted: 20 November 2022
Published: 6 December 2022

1. Introduction

The extraordinary optical, mechanical, electrical, and temperature characteristics of graphene make it a unique material. Recently, graphene-based nanostructures have attracted significant attention. Graphene is a honeycomb-shaped bilayer (2D) sheet of carbon particles. Other graphene structures, such as graphene oxide (GO) and reduced graphene oxide (rGO), are also being explored because of their wide range of applications in sensors, energy capacity, water sanitization, optoelectronics, and other fields. Therefore, it is important to understand the difference between GO and rGO. Graphene oxide is synthetically modified graphene. Shedding and oxidation are used to synthesize GO, which is associated with a significant adjustment of the basal plane in its structure. The monolayer GO films had a high oxygen content. The carbon/oxygen ratio of GO is often below 3:1 and close to 2:1.

Numerous investigations on the environmental applications of GO–metal-based hybrids have been published in the last decade, but the literature is replete with contradictory reports of their performance. These deviations are due in part to the highly variable nature of the synthesis methods of GM hybrid materials. The surface chemistry, lateral size, and crystalline structure of GM hybrids are predominantly dependent on the synthesis methods. Similarly, the pore size distribution and interlayer spacing can also be affected by the synthesis methods. Furthermore, half-breeds of GO/rGO with metal/metal oxide nanostructures had synergistic attributes [1].

We critically review recent advances in the ecological application of GM hybrids. Most GM hybrids fabricated for water treatment are 2D and 3D materials, typically GO–metal composites, membranes, or three-dimensional matrices, in addition to a polymer. The

main objective of this review is to highlight the link between the material properties of GM hybrids and their environmental performance. Graphene has high carrier mobility, outstanding mechanical strength and flexibility, high thermal conductivity, a large specific surface area, and excellent electrical conductivity [2]. Figure 1 shows the graphical illustration of GM hybrids in various environmental applications.

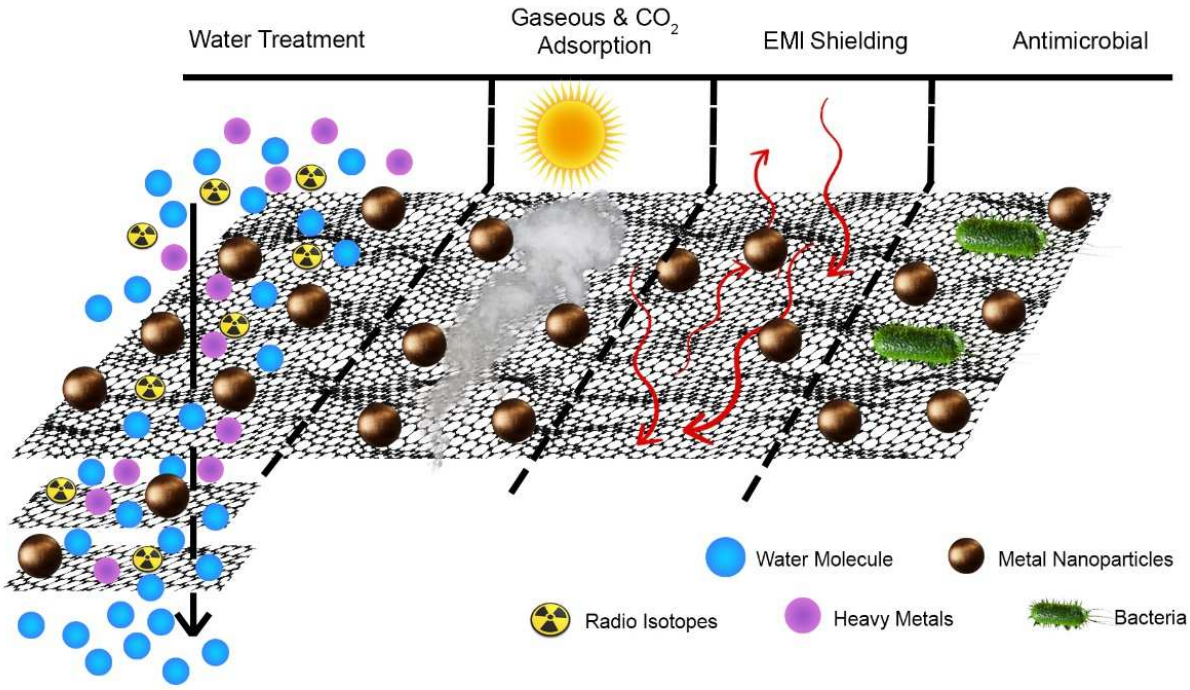

Figure 1. Schematic illustration of graphene oxide hybrids for environmental applications in water purification, gaseous CO_2 adsorption, electromagnetic shielding, and antimicrobial elimination.

2. Architecture of Graphene Oxide–Metal Nanocomposites

The surfaces of graphene oxide are partially hydrophobic with hydrophilic regions with potential for hydrogen bonding and metal ion complexation and contain negative charges at the edges associated with carboxylate groups. Furthermore, graphene oxide contains aromatic domains (sp^2) and (sp^3), leading to an increase in the types of interaction that can occur on the surface. The long-term stability of GO in saline or a culture medium requires additional functionalization. The edges of GO are rich in carboxyl groups (-COOH), whereas the hydroxyl (OH) and epoxy (=O) groups are abundant in the basal plane. Understanding the chemical and physical properties of the metal/graphene oxide (M/GO) interface is essential for the use of GO in practical applications because the metal layer must be securely attached to GO [3]. Metal permeation from the surface into GO at the M/GO interface can be detected at room temperature for metals such as Cu [4], Ag [5], Ni [6], Au [7], and Pd [8]. Graphene-oxide-based noble metal nanoparticles are exceptionally stable as two-dimensional (2D) graphene oxide substrates. The GO substrate served as a support structure for the metal nanoparticles (MNP), thus omitting the possibility of metal aggregation. These metals first become hydrated ions as a result of redox reactions (with GO reduction) near the surface, and subsequently permeate the interlayers. At normal temperatures, Au and Pt were observed to infiltrate GO as atoms in the GO bulk; however, permeation rates were slow [9]. Metal adhesion to graphene oxide (GO) is critical for the formation of adequate connections when GO or reduced GO (rGO) is used in electrical and electrochemical devices [10]. Furthermore, the metal–graphene oxide (M/GO) contact can act as a catalytic site for chemical processes.

Metal attachment was expected to have a significant impact on the concentration of oxygenated functional groups at this contact. Because defects and the content of oxygenated functional groups affect the properties of M/GO interfaces on the atomic and/or

electronic scales, understanding them on these scales may lead to the development of new electronic/spintronic, photochemical, and electrochemical devices. Metal sputtering on graphene and GO surfaces, however, damages and/or eliminates the top layer, while also changing the GO composition (through reduction). Compositional changes vary depending on the metal type, implying that some interactions occur between the metal and the GO surface. This permeability occurs at room temperature, particularly in humid environments, and there are two primary modes of metal ion/atom permeation [9]. The main type of metal immobilization on graphene oxide sheets is the general and widely used chemical reduction method, which is recognized as a green synthesis. Another study, for example, found that, CuO was self-assembled in rGO layers using NaOH as a reduction agent for application in supercapacitors [11]. In another example, the decoration of partially reduced graphene oxide with uniformly distributed AgNPs with an average size smaller than 4 nm was achieved by simultaneously reducing $AgNO_3$ and GO in the presence of ascorbic acid [12]. A new graphene–copper nanoparticle composite was prepared by chemical reduction in situ of a mixture containing graphene oxide and copper (II) ions using potassium borohydride as a reducing agent [13]. In contrast, in the absence of any stabilizer, GO–AgNP nanohybrids have been effectively produced using an environmentally friendly one-step method for antibacterial applications [14]. One of the major advantages of solution processing is the self-assembly of metals onto the surface of GO, and the relative ease of synthesis and scale-up for commercial industrial use.

3. Environmental Applications of Graphene Oxide

3.1. Water Purification

3.1.1. Removal of Heavy Metals

The toxicity of heavy metals in the environment, such as Pb, Ca, Cu, Zn, Cr, Hg, Ni, Li, Fe, As, and Cd, induces toxicity to the ecosystem. Graphene oxide and its composites are beneficial for the removal of organic pollutants and microbes from contaminated waters because of their large surface area and high catalytic efficiency. Consequently, the literature reports that the adsorption process is one of the most effective methods to remove heavy metals from the complex water matrix of the other methods available [15]. Heavy metal adsorption by graphene oxide nanocomposites involves physical adsorption [16], chemical adsorption, and electrostatic interaction [17]. The interaction of graphene oxide with heavy metals usually occurs through precipitation, ion exchange, and surface complexation. Ununiform active sites on the evacuated surface of GO promote calcium ion adsorption from hard underground water [18]. The selectivity of graphene oxide for heavy metals in a complex matrix composed of dissolved organic matter and other contaminants was investigated by Jun et al. [19]. Negatively charged ion-chelating functional groups in GO induce nanocomposites based on graphene oxide, ideal for the removal of heavy metals, such as Cr (VI), Cu (II), Pb (II), and Cd (II), by chemical adsorption from the water matrix, as confirmed by the Langmuir model [20]. For the adequate removal of the heavy metals of greatest environmental concern in complex matrices, the limitations of graphene oxide, such as low sorption selectivity and difficulty in solid–liquid separation, can be improved by doping with metal nanoparticles. As an example, to enhance the selectivity of the heavy metal adsorption of Pb (II), graphene oxide hydrated manganese oxide nanocomposites (HMO@GO) were investigated [21]. Silver nanoparticles were produced on the GO sheets via the chemical reduction of Ag^+ ions on the GO surface. The fabricated Ag-GO was used as an adsorbent for malachite green (MG) and ethyl violet (EV) dyes, catalyst, and antibacterial agent by Hina et al. [22]. The functionalization of graphene oxide surfaces with more oxygen functional groups increased the adsorption capacity. Usually, oxygen functional groups are preferred for the removal of heavy metals because the negative surface charge of graphene oxide along with the negative surface charge of oxygen functional groups can aid in the efficient adsorption of positively charged heavy metals.

The use of magnetic materials in solid-phase extraction has received considerable attention considering the advantages arising from the inherent characteristics of magnetic particles. The choice of an appropriate magnetic adsorbent material dominates the selectivity and sensitivity of the method through hydrophobic interactions and hydrogen bonding. For example, Zahra et al. fabricated a reusable double-charged ionic liquid-modified magnetic graphene oxide (DIL-MGO) and applied it to the separation and preconcentration of Pb (II), Cd (II), Ni (II), Cu (II), and Cr (III). In addition to the higher adsorption efficiency, this compound (DIL-MGO) was also tested for the reclamation of these metals, which can add value to the reusability of the material [23]. Yue et al. synthesized self-propelled tubular motors containing an outer layer of graphene oxide and an inner layer of platinum as a catalyst that works under the influence of a magnetic field to remove lead from microchannels [24]. Subsequently, oxygen-rich functional groups allow graphene oxide to perform a secondary functionalization of GO for the preparation of hybrid nanomaterials. The formation of oxygen-containing functional groups in GO and its subsequent influence on its structure play a significant role in the adsorption and co-adsorption of polar and non-polar organics in fluid arrangements.

The higher adsorption sites in hybrids, achieved by suppressing particle aggregation and lowering the size of copper nanoparticles, explain the superior removal capabilities compared to bare particles [25]. Moreover, the structure of GO plays a significant role in providing access to active sites for the adsorption and regeneration of heavy metals. For example, Archana et al. [26] grafted NiO crystals onto graphene oxide sheets by hydrothermal treatment. The surface morphology of GO-NiO showed a substantial amount of space and surface wrinkles in a functionalized three-dimensional structure, resulting in greater accessibility to the active sites for the chemisorption of Pb (II) and Cd (II). The removal of selenium by water-dispersible magnetic graphene oxide nanocomposites was explored by You et al., 2014 [27].

3.1.2. Removal of DYE and Removal of Organic Pollutants

Many GO-based nanocomposites have been successfully used to adsorb metals and dyes from contaminated water. Similarly, for the adsorption of heavy metals, the availability of active sites and the ion exchange ability of GO for dye adsorption are key factors controlling the dye uptake capacity of graphene oxide composites. Moreover, the structure of graphene oxide and the porosity of GO also play a major role. Interesting research by Cecilia et al. [28] synthesized reoxidized GO (Ox-GO) by the modified Hummers method and evaluated the adsorption of methylene blue (MB) and rhodamine B (RB). The oxidized morphology of GO (Ox-GO) appeared to be more porous with an improved interlayer spacing, as determined by SEM. The presence of increased C=C, C–O, O–C=O, π–π, and π–π* in Ox-GO compared to graphene oxide was confirmed by XPS analysis. The MB adsorption capacity of Ox-GO was 30% higher than that of graphene, and the adsorption of RB was 40% higher than that of GO. Fu et al. reported that adsorption is strongly pH-dependent and ionic-strength-dependent, indicating an ion-exchange-based adsorption mechanism [29].

The cationic dyes were better adsorbed on the surface of GO, whereas the anionic dyes were better adsorbed on the graphene surface [30,31]. It was determined that this adsorption behaviour was caused by charge–charge interactions. Charge transfer occurs between negatively charged GO and dye molecules in the case of cationic dyes, whereas it occurs between negatively charged dye molecules and graphene species in the case of anionic dyes. Recently, H et al. [32] developed graphene oxide Au nanocomposites for the adsorption of ethyl violet (EV) and malachite green (MG) and catalytic reduction of 2-nitroaniline (cationic and anionic dyes). The π–π interaction between the hybridized carbon domains of sp^2 and aromatic dyes, as well as the electrostatic interaction between negatively charged nitrogen atoms and positively charged carbon of the dyes and Au nanoparticles, induced a better adsorption of approximately 77.82 mg/g and 30 mg/g for MG and EV, respectively.

Over a broad pH range, GO demonstrated excellent adsorption capabilities for Cd, naphthalene, and 1-naphthol. Additionally, the 1-naphthol -OH groups and the electron-depleted sites on graphene nanosheets show a larger adsorption range [19]. However, contact with other complexes present in the natural matrix of the environment, such as humic and fulvic acids, affects the environmental performance of the composites. Zhang et al. [33] tested magnetic graphene oxide nanocomposites for the removal of HA/FA and Pb (II) from landfill leachate with the regeneration capacity of the adsorbent for up to three cycles. The adsorption capacity of HA/FA for magnetic graphene oxide increased with an increase in the Pb (II) concentration. Similarly, the discharge of pharmaceutical products can be classified as an organic pollutant. Yang et al. [34] tested the adsorption of pharmaceutical products such as enrofloxacin (ENF) and rhodamine B (RhB) by graphene oxide (GO). Studies have shown that GO can remove approximately 92.5% of both RhB and ENF, along with recyclability for four cycles. A notable issue in the removal of dyes from natural matrices should be focused on, as laboratory systems cannot reflect real-life scenarios. Pervez et al. reported the sustainable synthesis of Fe_3O_4@GO + $K_2S_2O_8$ (persulfate-activated) with a degradation efficiency of Rhodamine B (RhB) of approximately 95% compared to Fe_3O_4 (≈25%) over a wide range of pH values [35]. Similarly, rGO/Fe_3O_4 has been used to remove methylene blue from contaminated water with an adsorption capacity of 75.15 mmol/g [36]. Moreover, there was a similar study with GO/Fe_3O_4 for the removal of Chrysoidine Y from contaminated waters with an adsorption rate of 344.83 mg/g [37]. By catalytic oxidation and photodegradation, metal oxides can mineralize volatile organic molecules, including benzene, ethylbenzene, toluene, and xylenes (BETX) [38,39].

Because a wide variety of nanosorbents are available, mathematical modeling, such as artificial neural networks, can be adapted to design study experiments that can improve the time frame of an experiment. Xin et al. studied the adsorption behavior of the mesoporous nanocomposite rGO/Fe/Cu in carmine and binary dyes (carmine and Congo red). The authors compared the predicted and experimental results using a backpropagation (BP) algorithm with input parameters such as dye concentration, pH, reaction time, and dose. The results predicted by the particle swarm optimization (PSO), genetic algorithm (GA), and the ox-Behnken design (BBD) were compared with the experimental adsorption results. ANN-PSO fits well with the experimental and predicted results. The experimental results were shown in 1848.96 mg/g of adsorption using the Langmuir isothermal adsorption model [40].

In addition to nanocomposites, polymeric membranes, sponges, and porous structures have also been used for the removal of dyes and organic pollutants. Likewise, the doping of metal carbides has been explored. Chandra et al. reported a mixed matrix membrane composed of copper–sulfur nanocomposites decorated with nitrogenated graphene oxide (CuxS-NrGO, where x = 1 and 2) on a polysulfone matrix. The authors examined the impact of a Congo red rejection of approximately 93%. Insignificant leaching of the nanoparticles was observed in CuxS-NrGO-incorporated PSF nanoparticles, which demonstrated robust contact between the N-active sites of NrGO, CuxS, and the N-active sites of the polysulfone matrix [41]. Kanani et al. reported the synthesis of magnetic manganese graphene oxide ($MnFe_2O_4$-GO) for the adsorption of the rhodamine 6G dye from aqueous solutions. The results showed that the absorption capacity of $MnFe_2O_4$-GO was 24.96 mg/g, while that of unmodified GO was 14.82 mg/g [42]. Gulzar et al. synthesized ZnO-GO nanocomposites for the photocatalytic degradation of o-xylene in water. The pH played an important role in the synthesis of the ZnO nanoflowers, and structural morphology analysis showed that the GO sheets were wrapped onto the 3D surface of the ZnO nanoflowers. The photocatalytic activity of the ZnO-GO composites for the degradation of ZnO-GO composites for o-xylene was 15% higher than that of ZnO flowers [43]. Jia-Hao studied the effect of Cu^{2+} on the adsorption of phenol-4-sulfonic acid (PSA) by TiO_2/rGO. The chemical stability of PSA has improved considerably in the presence of Cu^{2+} ions in wastewater [44]. The ultra-large surface area of graphene oxide has a significant contribution in the adsorption of dyes from

the environment. With increase in the surface area of graphene oxide–metal hybrids, the removal capacity of methylene blue increases as well (Figure 2).

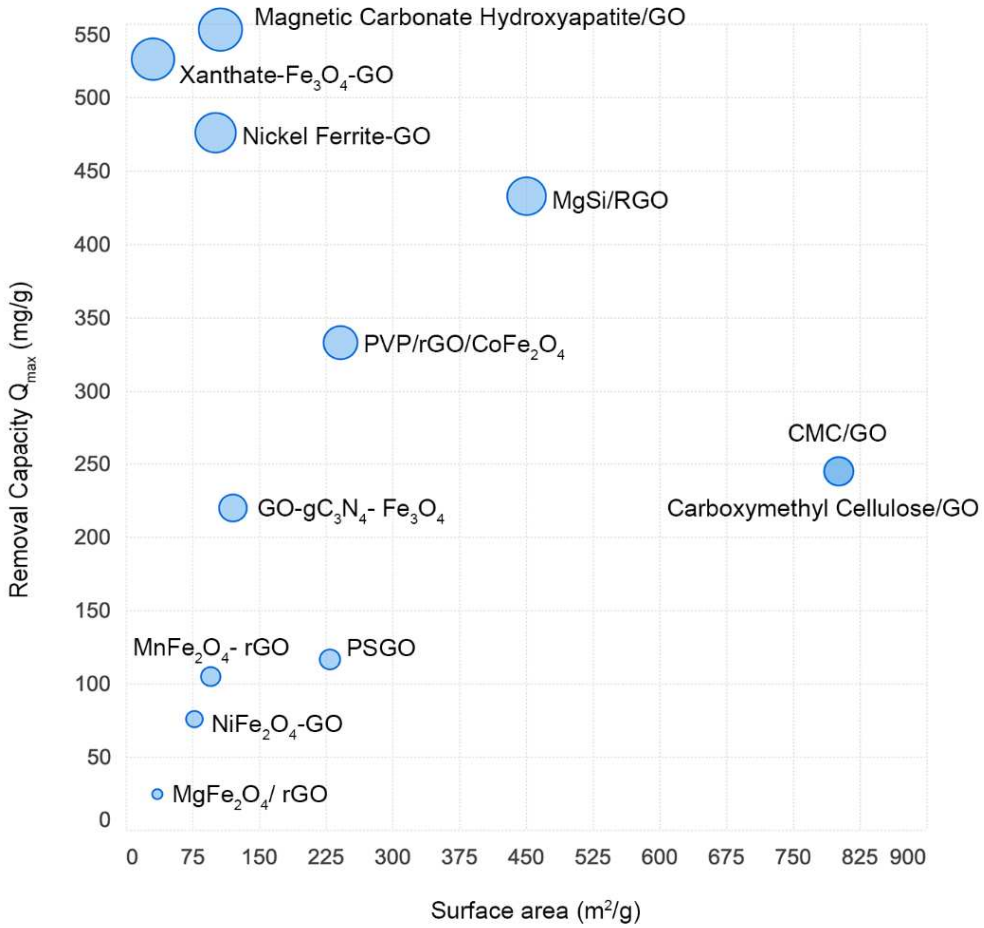

Figure 2. Removal efficiency of heavy metals by various graphene oxide–metal hybrids.

3.1.3. Removal of Radioisotopes

Although significant research has been conducted on the adsorption of radionuclides by graphene-oxide-based sorbents, the mechanism of interaction remains unclear [45–48]. The mechanisms of the adsorption and interaction of Am (III)/Eu (III), Cs (I), and U (VI) on defective graphene oxide were well explained by Kuzenkova et al. [49]. They created graphene oxide using a variety of synthesis techniques, including Hummer's, Brodie's, and Tour's methods (HGO, BGO, and TGO). In accordance with the adsorption results, Am (III)/Eu (III) and U (VI) interacted with carboxylic groups. Additionally, DFT calculations and the analysis of EXAFS and HERFD-XANES spectra revealed that radionuclides mostly fill vacancy defects in the GO sheets. Another research that correlates with Kuzenkova et al., by Nicolas et al., proposed an extremely defect-rich GO (dGO) for efficient sorption of U (VI) and Am (III). dGO showed a maximum adsorption capacity of Q_{max} = 2250 mmol/g at pH 5.1. This was due to the bonding of uranyl cations to carboxylic groups inside the defects in the GO structure [50]. Thermal expansion was followed by oxidation with ammonium persulfate and nitric acid. Unlike dGO, 3D GO showed a lower U (VI) adsorption capacity of 1950 µmol/g. This was attributed to pore collapse with the oxidation step followed by thermal expansion [51]. Therefore, mild oxidation of the material may be more logical without compromising the porous structure, or treatment of the material before the thermal expansion step might be more logical.

Magnetite GO nanocomposites are used in this process to remove harmful contaminants, such as radionuclides, uranium, thorium, and dyes [52–55]. Graphene-oxide-based nanocomposites have been effectively used for the adsorption of Pb, Co, Ni, and uranium

(U). Reduced zero-valent graphene-oxide-supported nanoscale iron has been used for the adsorption of radioactive U (VI) [56]. GO-based nanocomposites are the first choice for binding organic molecules, which is mainly attributed to their large surface area and reactivity. GO exhibits very strong π-stacking with a benzene ring, making it an ideal candidate for the removal of organic compounds from contaminated water. However, ion exchange and chemical reduction processes may also play an important role. The specific surface area of GO aids in the removal of radioisotopes, such as Th (IV), Pu (IV), Am (III), Eu (III), U (VI), Sr (II), Tc (VII), and Np (V) from the stimulated nuclear waste solution [57].

Manganese oxide (MnO_2) has a high adsorption capability to remove heavy metal ions and Th (IV) ions from wastewater due to its low cost, wide surface area, moderate oxidation, and good stability under acidic conditions. Xiu et al. [58] used the oxygen groups of the graphene oxide nanoribbons to attach a manganese dioxide composite material (MnO_2-GONRs) for the removal of Th (IV). A maximum adsorption capacity of 166.11 mg was observed at pH 3. Thermodynamically, this process was spontaneously endothermic. Another study showed that graphene oxide removes some of the most toxic and radioactive long-lived human-made radionuclides from contaminated water, even acidic solutions with pH values below 2.0 [49].

Amidoximated magnetite/graphene oxide compounds were used to adsorb U (VI) ions, and it was noted that U (VI) ions were adsorbed on the surface of AOMGO with an increase in pH. Briefly, the H^+ ions emitted by coordination reactions decrease repulsion between U^{2+} and AOMGO compounds through the deprotonation of functional groups, thus promoting sorption [59]. Imprinted GO-SiO_2 were used in a polymer to adsorb U (VI) at pH 4 because it showed higher affinity. pH is a vital parameter for the efficient uptake of radioactive elements into oxidized graphene oxide [60]. Recent research by Ehab et al. found the sorption of $^{152+154}$Eu in a graphene oxide composite. As the pH increased from 1.5 to 5.5, the adsorption capacity increased by up to 99%. The M-GO nanocomposites were synthesized using a coprecipitation method for the removal of Sr (II) and Cs (I) [61]. The Q_{max} values for Sr (II) and Cs(I) were 2.103 mg/g (based on the Freundlich model) and 142.070 mg/g based on the Dubinin–Radushkevich model), respectively, proving that the adsorption parameter is temperature-dependent, and M-GO follows physical adsorption [62]. The Cs^+ cations were better transport inhibitors at higher concentrations than most monovalent cations. GO can form inner-sphere complexes with Cs^+ and U (VI) [63–65].

Polyoxometalates (POMs) are anionic metal clusters consisting of tungsten, molybdenum, and niobium in higher oxidation states [66]. Yayu et al. incorporated platinum-based metalates, a new supersodalite cage that contains approximately spherical cavities, for the first time [67]. The idea of using a POM-based GO compound for the adsorption of Cs were investigated, since GO [68] and POM have been used to study the adsorption of Cs by the cation exchange mechanism [69]. Seino et al. proposed a reduction-induced highly selective uptake of Cs ions by silicododecamolybdate [70]. Nugroho et al. found that the incorporation of α-$K_6P_2W_{18}O6_2$ POM can improve the oxidized zone (sp^2/sp^3 hybrid carbon) of graphene oxide. Additionally, Dawson-type POM in the GO system improved the negative charge of the GO portion in the composite and allowed for effective Cs^+ ion adsorption. In conclusion, Q_{max} was 41.3 (mmol/g) for $[GO_{40}POM]_{41}$ at an initial concentration of Cs = 3.6 mmol [68]. Lujanienė et al. synthesized magnetic-GO for the adsorption of Pu and Am. They concluded that sorption activity depends on the availability of sorption sites for GO and magnetite, where, compared to MGO1, the MGO2 sorbent showed an improved adsorption capacity of about 100% for Pu and Am, since magnetite nanoparticles were evenly distributed on GO [54].

In most cases, adsorption reactions occur in a simulated water environment. Lujanienė et al. used magnetite–prussian blue–graphene oxide nanocomposites (MPBGO) nanocomposites for the removal of Cs (I) from contaminated water (362 mg/g) by physisorption. Moreover, MPBGO showed a 100% adsorption efficiency of Cs (I) from seawater in the presence of K^+, Na^+, and other ions [53].

Qian et al. explored the oxygen groups of GO [71]. However, the adsorption of short-lived radioisotopes used in radiopharmaceutical applications has not been extensively explored. Unique research by Mohammed et al. used graphene oxide for the chemical adsorption of fluorine-18 fluorodeoxyglucose (^{18}F-FDG) with a half-life of 1.83 h. Chemisorption occurs due to the presence of nanolayers ($\pi \rightarrow \pi^*$), and the surface area of GO wraps around, resulting in the adsorption of ^{18}F-FDG. This work may contribute to the development of new graphene-oxide-based adsorbents with applications in hospital radio waste [72].

Graphene oxide (GO) is a carbonaceous layered substance rich in oxygen that has a higher adsorption limit and is more scattered in water than graphene. Accordingly, GO can be a powerful adsorbent for the removal of uranium. Although numerous exploratory studies have focused on the adsorption of uranyl on GO, further examination is required at the subatomic level to comprehend the underlying holding nature and communication components of GO/uranyl, particularly from a hypothetical outlook. The limiting directions and electronic attributes of uranyl particles are subject to a growing number of hypothetical reproductions.

3.2. Adsorption Equilibrium Parameters of Uranium Ions

The adsorption capacity increases with increasing temperature, mainly because the rate of diffusion, both internal and external, increases with increasing temperature. Uranium is an actinide element that is widely used in most nuclear reactors and is an important contributor to nuclear waste. The surface functional groups of GO-based nanoparticles are primarily responsible for their strong uranium adsorption. Because of the variety of functional groups on GO-based nanomaterials, the effect of different functional groups on uranium adsorption is unknown. Here, we attempt to correlate the adsorption parameters of materials with the adsorption of uranium. In general, sorption parameters provide information on the mechanisms involved in the adsorption process. Thermodynamic parameters, such as the Gibbs free energy change (ΔG), enthalpy change (ΔH), and the entropy change (ΔS), were calculated from temperature-dependent sorption data. The sorption of radionuclides onto GO-based materials is an endothermic and spontaneous process. The sorption of uranium on GO is influenced by the solution conditions, ionic strength, experimental conditions, pH, and temperature. Because of the thermodynamic parameters at different concentrations of the GO adsorbate and the U adsorbent, finding a correlation between entropy and enthalpy is not reasonable. In general, enthalpy–entropy compensation is present only when ΔG^0 is constant. Changes in Gibbs free energy and entropy were estimated based on temperature-dependent equilibrium constants. Figure 3 shows the enthalpy versus entropy compensation effect of GO-M hybrids on adsorption of uranium adsorbates and Figure 4 shows the temperature vs. pH of GO-M hybrid adsorbents of uranium adsorbates (see application in Tables 1–7).

3.3. CO_2 Capture

Graphene oxide can effectively remove gaseous contaminants in a manner similar to that of contaminant removal from water. Graphene oxide has been previously investigated for its potential in CO_2 capture and its electrochemical, thermal, or photocatalytic reduction to CO. The resulting CO, CH_3OH, CH_2O, HCOOH, and C_3H_8O were used as precursors for fuel and chemicals. Like the removal of impurities from water, GO can remove gaseous contaminants. Graphene-based materials are known for their potential in CO_2 capture and their electrochemical or photocatalytic reduction to CO.

Under powerful adsorption/desorption conditions, rGO can be used as an adsorbent for volatile organic compounds (at ppm levels) [73,74]. The adsorption capacity of graphene oxide is increased with increasing temperature, pressure, interlayer distance, and the addition of nitrogen compounds. As a most striking example, nitrogen-doped reduced graphene oxide (NRGO) exhibited the highest specificity for CO_2, with 3.81295232 ($g \cdot g^{-1}$) maximum specific absorbance of 3.81295232 $g \cdot g^{-1}$ and a specific surface area of 9916.88239 m^2/g [75].

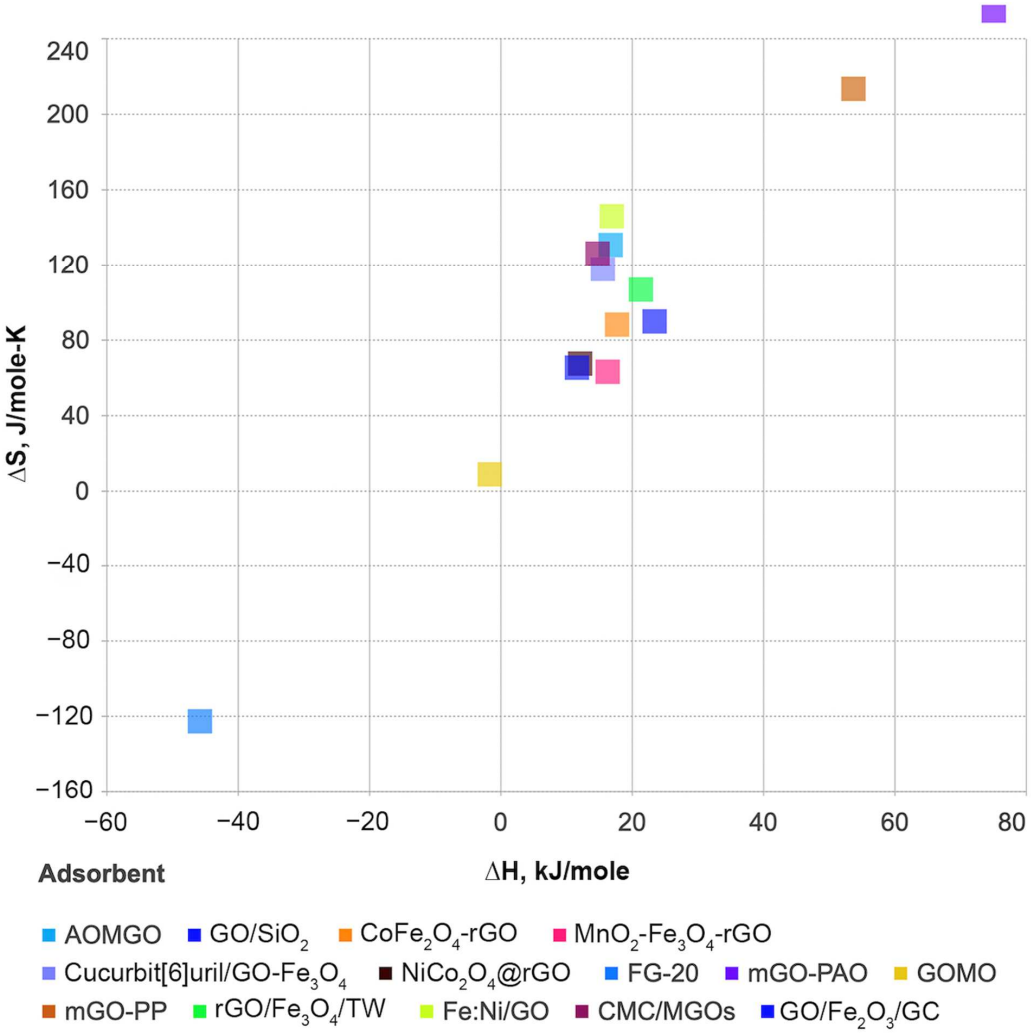

Figure 3. Enthalpy vs. Entropy compensation effect of GO-M hybrids on adsorption of uranium adsorbates. Data listed in Table 5.

The performance of graphene oxide can be improved by decorating it with catalytic nanomaterials [76]. Moreover, to improve the governing factors influencing the removal efficiency, surface chemistry can be improved by decorating the GO surface with reactive nanomaterials. Several metals and metal oxides exhibit excellent bandgap, electrical conductivity, and stability under experimental conditions. CO_2 capture can be greatly influenced by catalyst, catalyst carrier, and integration strategies. Different nanoparticles with catalytic properties can be used for CO_2 capture, such as copper [77].

The photocatalytic reduction of CO_2 requires several electron transfers and can produce a wide range of products depending on the precise reaction pathway adopted and the number of electrons transferred, which determine the final oxidation state of the carbon atom. The photocatalytic reduction of CO_2 can be achieved using various metal composites. Graphene has shown potential as an effective electron acceptor and transporter for photocatalytic CO_2 reduction and reduces photogenerated charge carrier recombination. A study demonstrated the photocatalytic reduction of CO_2 in methanol (CH_3OH) and methane (CH_4) using silver chromate (Ag_2CrO_4) nanoparticles as photosensitizers and graphene oxide (GO) as cocatalysts. They concluded that, as a cocatalyst, GO assisted in charge transfer and improved CO_2 adsorption and catalytic sites [78]. TiO_2 and its photocatalytic ability to reduce CO_2 have been extensively studied. Due to its extensive 3.2 eV band gap and excellent efficient photoactivity, high stability, and low cost, graphene oxide can be used for excellent CO_2 reduction [79]. A vertically aligned TiO_2 nanostructure-wrapped GO/rGO

layer were used for the photocatalytic reduction of CO_2 to CO. The unique morphology with graphene oxide as a cocatalyst combined with TiO_2 as a photocatalyst resulted in a maximum CO yield of 1348 µmol/g (Figure 5C) [80]. Indrajit et al. synthesized GO-Cu nanocomposites via a one-pot microwave process. The compound developed has a strong interaction between copper nanoparticles and graphene oxide, which helps to produce higher CO_2 of approximately 6.84 $\mu mol/g_{cat-1}h^{-1}$ for the reduction of photocatalytic CO_2 under visible-light irradiation [81] (Figure 5A). Solvothermal methods and subsequent photochemical deposition have been used to successfully create Ag-RGO-CdS nanocomposites. Zezhou et al. implemented Ag-RGO-CdS for the catalytic conversion of CO_2 to CO in a photocatalytic system with TEOA as a hole scavenger. As a result, 1.0 wt.%-Ag3.0 wt% RGO-CdS presents the highest photocatalytic performance of 1.61 µmol/h in comparison with bare CdS nanorods (0.21 µmol/h) (Figure 5B) [82]. Deerattrakul et al. synthesized Cu-Zn/reduced graphene oxide (rGO) catalysts by incipient wetness impregnation and estimated the hydrogenation of CO_2 to methanol using a fixed-bed tubular stainless-steel reactor. As a result, 424 $mg_{MeOH}\ g_{cat-1}h^{-1}$ of methanol was obtained at 250 °C with a loading content of 10 wt% Cu-Zn metals on rGO [83]. In general, a catalytic system requires an additional sacrificial donor for the photoreduction of CO_2, resulting in efficient fuel generation from CO_2. To overcome this, Tingting et al. synthesized nitrogen-doped graphene (Gr–CuC) for CO_2 in methanol under visible-light irradiation [84].

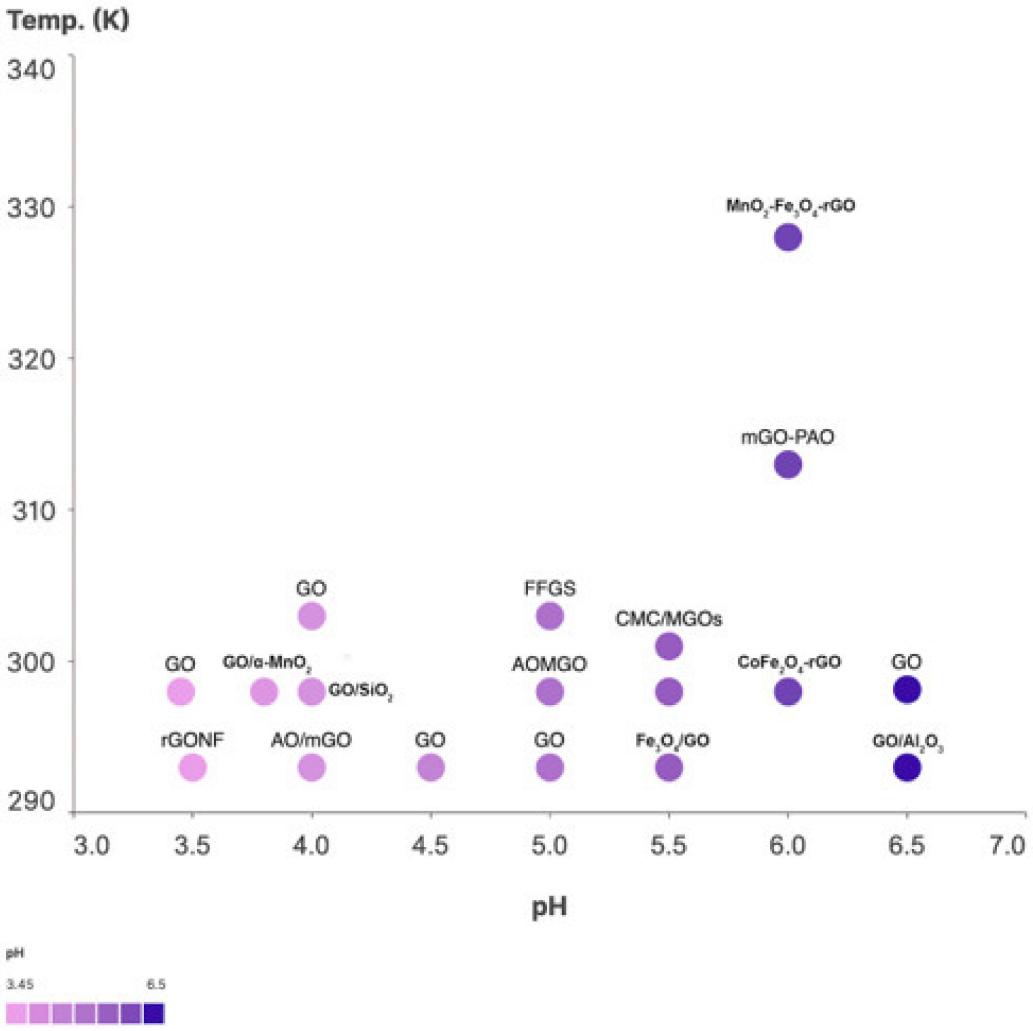

Figure 4. Temperature vs. pH of GO-M hybrid adsorbents of uranium adsorbates. Data listed in Table 6.

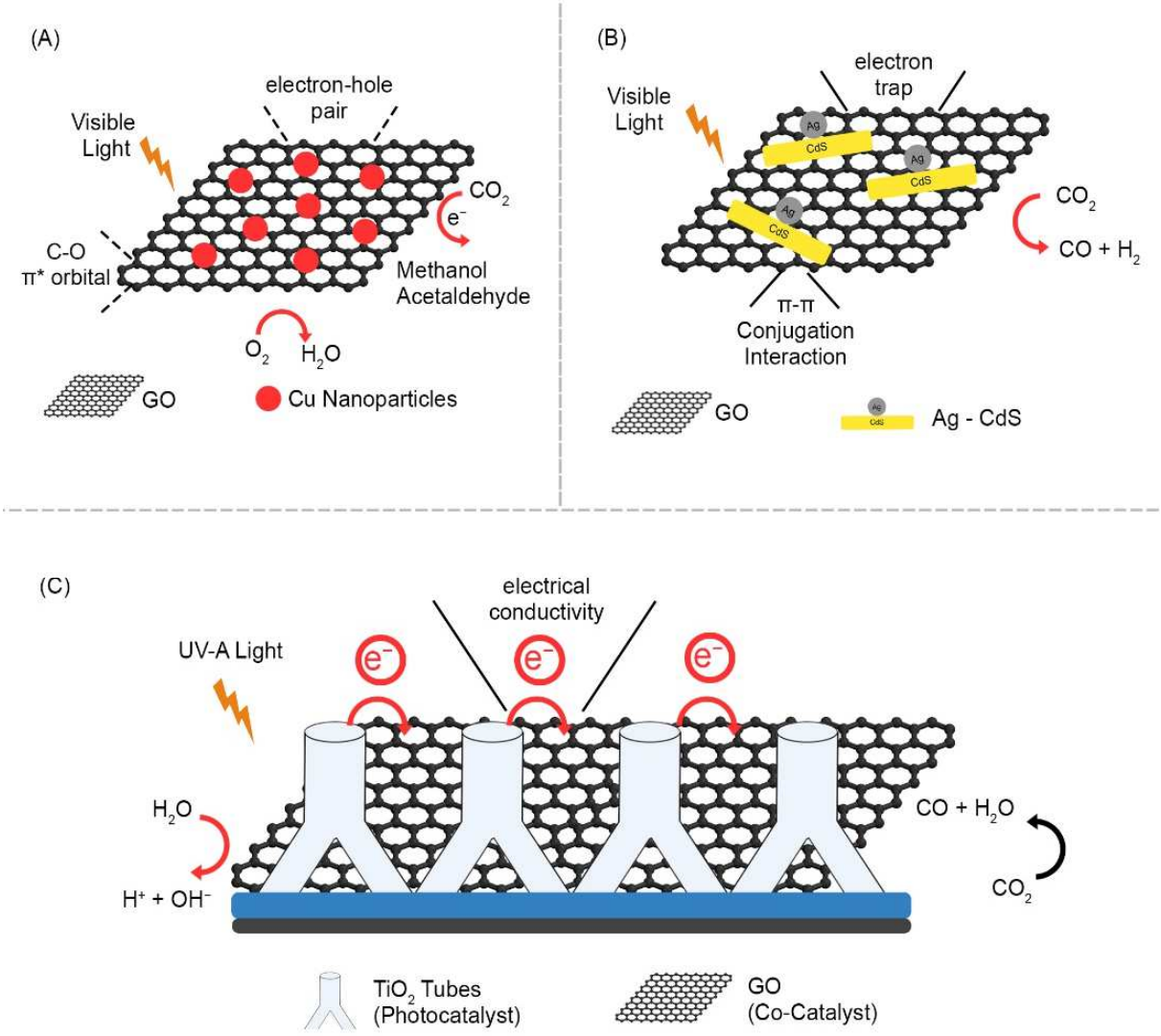

Figure 5. Mechanism of CO_2 reduction in GO metal hybrids: (**A**) Cu [81]; (**B**) Ag-Cds [82]; (**C**) TiO_2 [80].

Similarly, to minimize the overpotential of CO_2 reduction, electrocatalysts are needed in the catalytic process known as electrocatalysis, which involves reactions of oxidation and reduction by the direct transfer of electrons. The electrocatalytic CO_2 reduction reaction (CO_2RR) is an inner-sphere process in which adsorption and bond rearrangement, as well as reaction intermediates, take place inside the inner Helmholtz region (IHR). Several studies have been conducted to develop graphene oxide–metal hybrids with increased CO_2 reduction activity. Additionally, it was discovered that the rGO and CO_2 molecules interact via a π–π conjugation, which is crucial for facilitating adsorption and activating CO_2 molecules on the catalytic surface. Zhirong et al. synthesized porous In_2O_3 nanobelt-reduced graphene oxide (rGO) catalysts. To better understand the CO_2 reduction mechanism, DFT calculations were performed and compared with the experimental results. The results revealed that In_2O_3–rGO reduced CO_2 electroreduction by improving electrical conductivity and stabilizing the key intermediate $HCOO^{-*}$ [85]. Strong metal support contacts primarily contribute to improved electrochemical CO_2 reduction activity by improving interfacial electron transfer ability, according to experimental kinetic data. Zhang et.al., used rGO supported gold nanoparticles for electro catalytic reduction of CO_2 [86]. A lone pair of nitrogen electrons interacts with transition metal complexes to form composite materials [87].

CO_2 reduction using Pt-RGO catalysts was carried out in a novel, light-driven, electrically biased PEC cell with a Pt-TNT photoanode to successfully convert CO_2 into compounds such as C_2H_5OH and CH_3COOH. Under a 300 W Xe arc lamp as a light source, and a constant 2 V supply potential, the highest carbon atom conversion rate of 1130 nmol/(h·cm^2) was obtained with the Pt-RGO catalyst [88]. Nitrogen doping with graphene oxide has been extensively studied for CO_2 reduction, since the lone pair electron in nitrogen interacts with the transition metal complex and forms composite materials. For example, copper is complexed with nitrogen-doped graphene, where nitrogen doping is achieved using ethylenediamine as an additive. The team used GrN700–CuC to reduce CO_2 to methanol under visible-light irradiation. They reported a methanol yield of 1600 mmol/g·cat. Additionally, they proposed that the photosensitizing capacity of copper, along with the hybridization of nitrogen, resulted in enhanced electron transfer to improve the yield of methanol [89]. Moreover, the addition of metal organic frameworks is known to enhance CO_2 adsorption due to their tunable specific surface area and pore size by surface chemistry. The size of the pores and the interlayer space between the layers also play a vital role in CO_2 adsorption. CuBTC@GO was manufactured for the adsorption of N_2 and CO_2 using a mixed-solvent strategy. The material had extra porosity because of the interaction between CuBTC and GO, as the open metal sites in CuBTC can coordinate with the oxygen functional groups in GO, resulting in the formation of new pores. The material has a CO_2 adsorption capacity of 8.02 mmol/g at 273 K and 1 bar [90].

The catalytic conversion of CO_2 to Co and other organic compounds improves the catalytic activity of rGO [91]. Another study by Gunathilake et al. showed that increased CO_2 adsorption is due to the presence of terminal OH groups and acid–base pair sites on the magnesium surface ($Mg^{2+}O^2$) in MONP and MONP–GO materials, respectively, resulting in the formation of hydrogen carbonate species and bidentate carbonate complexes with CO_2 gas [92]. To better understand the role of oxygen functional groups in VOC [93], rGO was synthesized using hydrazine hydrate (N_2H_4) as a reducing agent and made on silver electrodes using the drop casting method. The size of the pores plays an important role in the adsorption of pollutants in the gaseous phase. Lim et al. synthesized a thermally expanded graphene oxide powder with a pore size of approximately 5 to 25 nm with an adsorption capacity of toluene (92.7–98.3%) and xylene (96.7–98%) and reusability (91%). The adsorption capacities were found to be 691 cm^3/g for toluene and 191 cm^3/g for gaseous xylene, using the BET method. They concluded that the specific surface area, pore size, and oxygen functional groups present on the surface of the TEGAs improved its adsorption capacity [94].

Using a UV photocatalytic degradation–adsorption process, bismuth oxide nanoparticles linked to heterogeneous graphene/graphene oxide were employed to quickly remove xylene vapor from ambient air (BONPs-NG/NGO). The adsorption capacities of xylene with 200 mg of BONP-NG/NGO and NG/NGO were 223 mg/g and 134.6 mg/g, respectively, at 85 °C for 10 min [95]. Because most CO_2 reduction occurs in the laboratory, under controlled conditions, we cannot fully understand the dynamics of the material in real-time applications. Mateo and his colleagues, for photoassisted reduction of CO_2 with H_2O, studied the photocatalytic activity of NiO/Ni nanoparticles (NPs) supported on flawed graphene (NiO/Ni-G) under air. The photocatalytic reduction process was carried out in a reactor at a pressure of 1.3 bar, and the illumination was a 300 W Xe lamp. As a result, NiO/Ni on graphene promotes photoassisted CO_2 methanation at 642 µmol/g·h at 200 °C under continuous flow at a rate of 244.8 µL/h [96].

3.4. Electromagnetic Interference (EMI)

Interestingly, adaptable graphite has been utilized as an electromagnetic interference (EMI) protective material. The peeled graphite pieces were packed without fasteners to produce adaptable graphite sheets with a decent and large surface region. The EMI of adaptable graphite was estimated using the coaxial transmission technique at frequencies in the range of 1 to 2 GHz. The creators determined that the EMI SE of adaptable graphite

was extremely high with this L-band recurrence. Regardless of its use for EMI safeguarding, adaptable graphite can also be utilized as an EMI gasket material because of its toughness. Given its high similarity to natural polymers, GO can be utilized as an engaging nanofiller in polymer nanocomposites, extensively developing the electrical, mechanical, and warm qualities of polymers. Furthermore, practical gatherings containing oxygen at the edges and bases of GO guide the expansion of the interfacial holding and the displacement of pressure from the polymer grid to polymer nanocomposites, resulting in polymer nanocomposites with prevalent support capacities [97]. Xu et al. synthesized large-scale thermally reduced graphene oxide films with an EMI shielding potential and high conductivity of 500 S/cm. Furthermore, the synthesized rGO sheets exhibited an excellent EMI SE of 45–54 dB, with a film thickness of less than 0.1 mm [98].

The exponential increase in the demand for electromagnetic interference shielding materials has led to the development of new shielding materials in recent years. Generally, an effective shielding material has three main functions: reflection, absorption, and multi-reflection. The high conductivity of graphene oxide (GO) makes it an ideal candidate for electromagnetic interference shielding. Multiple layers of graphene can hinder the optical transparency of a shielding material for applications in transparent films. Shi et al. proposed a cost-effective lithography technology to synthesize a four-layer graphene mesh with an even thickness. A uniform structure was achieved using an organic combination of microstructure patterning and continuous meshing. Compared to a two-layer graphene film, the four-layer graphene mesh showed a 1.26-time increase in absorption-based SE of 4.22 dB at 12–18 GHz, along with an improved transmittance efficiency of 95.26% [99]. Using adsorption as the dominant shielding mechanism, CuS/RGO compounds without any reducing agent from copper (II) dithiooxamide (Cu–DTO) and GO as a precursor were obtained via the hydrothermal method. Mechanical constancy is the priority to be assessed for the persistence of mechanical deformation in real-life applications. Using CuS as a pseudo capacitor and rGO as a conductor, a shielding efficiency of 64 dB at 2.3 GHz was achieved [100]. A novel nickel-foam-supported rGO(NI-rGO) foam was fabricated without any reducing agent. This foam is then pressed to a paper form by a hydraulic press at 20 MPa for 10 min, resulting in an RGN paper-like thin film by thermal annealing with a mechanical strain of 80% for 1000 cycles and enhanced shielding efficiency of 55 dB with 0.12 mm thickness, accompanied by a thermal conductivity of ≈247 W/(m·K) [101]. A noteworthy work by Hui Jia et al., investigated a free-standing GO/Ag nanowire (40 nm) film that covers the X-band, Ku-band, K-band, and the Ka band with an EMI shielding efficiency of 62 dB with a material thickness of 8 mm. The positively charged 1D silver nanowire with proven EMI shielding efficiency also favored the formation of the 3D conductive network via the vacuum-assisted self-assembly route of fabrication. The GO/Ag-7L demonstrated outstanding 62 dB performance in a frequency range of 8–40 GHz. This result suggests that the Ag nanowire boosted the conduction and tunnelling in the 3D GO layer of electrons without compromising the strain value with 5000 bending cycles [102]. FeNWs-rGO Fe_3O_4 nanowires were grown on rGO sheets using an in situ growth mechanism. The authors assembled Fe_3O_4 nanowires based on spatial confinement effects into vertical, parallel, and randomly assembled Fe_3O_4 NW onto the epoxy layer via an external magnetic field. Vertically aligned Fe_3O_4 NW showed an electrical conductivity of 37 S/m and improved shielding efficiency compared to parallel and randomly assembled Fe_3O_4 NW. This is due to charge accumulation from interfacial and dipole polarization by the hetero-interfaces formed by Fe_3O_4 NW-rGO. Moreover, increased polarization relaxation and dielectric loss, assisted by the external magnetic field, attenuate the EM wave [103].

Using the dielectric loss and magnetic loss mechanism of magnetic metal nanocomposites, Zhongji et al. used a two-step approach for developing loaded iron-cobalt-nickel oxide (FeCoNiOx) onto poly-dopamine-reduced graphene oxide. The FeCoNiOx-PDA-rGO composite possessed a reflection loss value of −36.28 dB at a thickness of 6.5 mm. The reflection loss value is achieved by the dielectric loss capacity of a defective graphene

surface, followed by the magnetic loss and dielectric loss mechanisms of metal and its oxides that help in the overindulgence of incident Em waves [104]. Graphene oxide for ionizing radiation was explored earlier [105,106]. Malinski et al. investigated the structural changes in irradiated GO surfaces with an energy of 40 keV using Au and GA ions and 500 keV helium and gallium ions. The irradiated GO foils were characterized by Rutherford backscattering spectrometry (RBS) and elastic recoil detection analysis (ERDA), which showed fluence of ion implantation and deoxygenation with modification of the GO surface. They also found that the modification of the elemental composition of GO after irradiation with 500 keV helium and gallium ions is due to nonelastic nuclear stopping and a low degree of GO deoxygenation [107,108].

Kumar et al. reported the thermal conductivity in the plane of rLGO (reduced large area GO) in-plane thermal conductivity (1390 W/m·K), high electrical conductivity (243 S/cm), and adequate EMI shielding effectiveness (~20 dB) through low-temperature chemical reduction using hydroiodic acid. The structural properties exhibited fewer defects in the sp^2 structure caused by the edge boundaries. This synthesis method showed enhanced electrical and thermal conductivities with CVD-produced single-layer graphene, making this synthesis approach a low-cost and mass-production candidate for applications in portable electronics [109]. Polyaniline as a polymer matrix, due to its lightweight and flexibility, has gained a great deal of attention in X-ray shielding applications, especially with fillers and additives [110]. Maryam et al. decorated GO with tungstic acid, bismuth sulfite, and tin (II) chloride, and then polymerized it with polyaniline and tungsten trioxide (PANi-W-G-TBT). They loaded a polymer matrix with 5 and 10 wt% hybrid GO flakes. The EMI shielding effectiveness of the PANi-W-G-TBT displayed an attenuation efficiency of almost 100% at a thickness of 40 KV 9 mm, which is caused by increased photoelectric absorption. This enhanced X-ray attenuation ability of PANi-W-G-TBT in the composite is due to its uniform distribution within the polymer matrix. Second, the probability of photoelectric interaction is proportional to the biquadrate of the adequate atomic number of the shields. This finding could lead to the development of lead-toxicity-free X-ray shielding material [111].

Aramid fibers (aromatic polyamide) are known to enhance the spacing between layers and minimize internal voids in composites by mechanical interlocking [112]. Xie et al. fabricated a robust hybrid aerogel from Ti_3C_2Tx/RGO/ANFs. The Ti_3C_2Tx/RGO/ANF aerogel was synthesized by fabricating a nanocomposite structure by mixing Ti_3C_2Tx flakes, GO sheets, and polyamide fibers, which were then freeze-dried, followed by thermal reduction at 400 °C. The resulting spongy aerogel with a load weight of 25% and a thickness of 2.6 mm reached a shielding efficiency of 54.8 dB X-band (8.2–12.4 GHz). This efficiency is due to multiple reflections of incident rays within the pores of the aerogel, complemented by ohmic loss, dipole, and interfacial polarization [113]. Figure 6 shows the EMI shielding efficiency of various GM metal hybrids.

3.5. Antimicrobial Activity

The innate antimicrobial properties of graphene oxide result from the physicochemical interactions of bacteria with oxygen-containing functional groups. This abundance of oxygen groups also assists in the hybridization of nanoparticles through electrostatic and coordinate approaches. AgNPs are known for an extensive range of antimicrobial studies against *E. coli* and *S. aureus*. Like graphene oxide, AgNPs also initiate cell death by damaging the cell membrane upon contact, producing reactive oxygen species, and interrupting ATP production. Stabilizing agents are typically used to prevent agglomeration and control its structure. Correspondingly, Mónica Cobos used an environmentally friendly approach to produce GO-AgNPs using a green reducing agent. GO-AgNPs were tested against *Escherichia coli*, *Pseudomonas aeruginosa*, and the Gram-positive bacterium *Staphylococcus aureus*. They concluded that the cytotoxicity of the nanohybrids depends on the smaller size of the silver particles, which have a larger surface area for bacterial

interaction. Furthermore, nanoparticles induce dose- and time-dependent toxicity against all microorganisms, especially *C. albicans* and *S. aureus*, and were studied by Neto et al. [14].

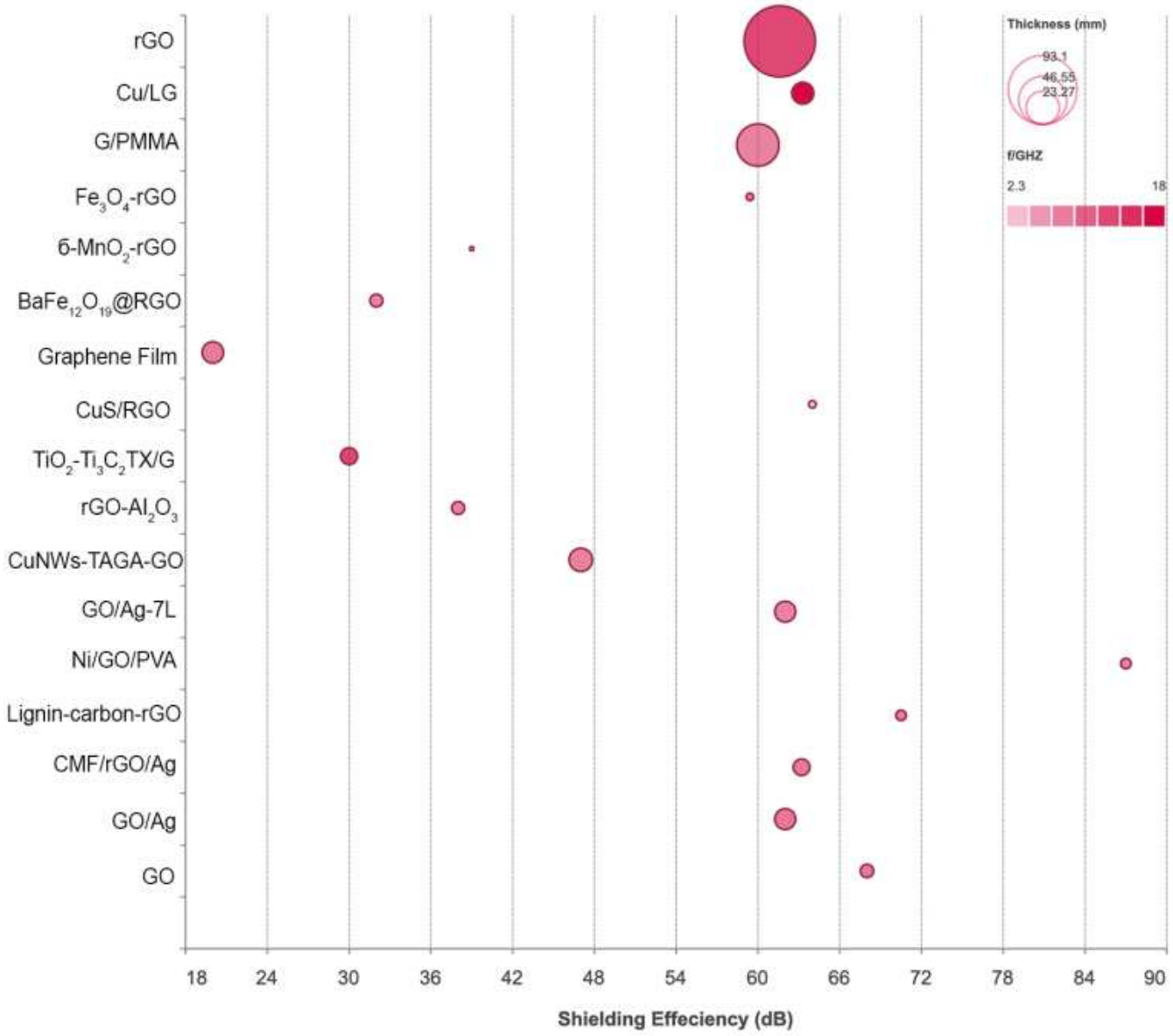

Figure 6. EMI shielding efficiency of GM metal hybrids. Data listed in Table 7.

Silver nanoparticles have gained considerable attention because of their variety of applications such as antimicrobial and medical applications over the years. Although the antibacterial property of silver nanoparticles has been exploited, the prevention of biofilms is still unclear. To test the inhibition property of biofilms on stainless-steel material (SS) used in medical procedures, Saravia et al. studied the antimicrobial property of *Pseudomonas aeruginosa* PAO 1, *Escherichia coli* (ATCC11229), *Acinetobacter* sp. (KM349193, NCBI-GenBank), *Bacillus cereus* (ATCC 10876), *Staphylococcus* sp., and *Kocuria rizophila* using the Kirby–Bauer method. *P. aeruginosa* and *K. rizophila* showed a higher sensibility towards Ag-GO nanoparticles on the SS material [114].

Moreover, the use of bimetallic nanoparticles with graphene oxide in the antibacterial field has recently been explored. Menazea et al. fabricated graphene oxide thin films decorated with silver and copper oxide nanoparticles. They prepared GO-Ag by adding $AgNO_3$ followed by NaOH to the water dispersion of GO and GO-CuO by adding $CuCl_2.2H_2O$ followed by NaOH to the water dispersion. These nanoparticles were tested against

Escherichia coli, and *Staphylococcus aureus* showed antibacterial inhibition comparable to that of *E. coli.* Antibacterial activity was examined against both Gram-positive bacteria (*Staphylococcus aureus* = *S. aureus*) and Gram-negative bacteria (*Escherichia coli* = *E. coli*) bacteria [115]. Subsequently, they continued to experiment with the same composites using the pulse ablation technique. Silver and copper nanoparticles were embedded into GO thin films using the laser ablation technique and tested against *E. coli* and *S. aureus*. The experiment concluded that the inhibition zone was 10.2 ± 1.1 mm against *E. coli* and 15.2 ± 1.6 mm against *S. aureus* [116]. In addition to silver, metallic zinc and zinc oxide particles have antibacterial properties. Considering the enhanced antibacterial effects described earlier, the addition of metallic oxides and metallic oxide nanoparticles to the GO sheets improved the antibacterial activity. Additionally, ZnO nanoparticles have shown good antibacterial activity when bacteria encounter ZnO ions along with disruption of the cell wall.

Chowdary et al. showed that ZnO can enhance the antibacterial effect of GO-chitosan sheets through ROS production [117]. The surface abrasiveness of ZnO when in contact with the surface of the bacterial cell membrane is assumed to be responsible for the high antibacterial activity of ZnO particles [118]. Moreover, the release of zinc ions from ZnO plays an important role in inducing the antibacterial activity of ZnO. ZnO particles of approximately 4 nm in size were anchored homogeneously against thin GO films, and antibacterial tests were performed. The zinc ions of zinc acetate react with the oxygen groups of the GO sheets via electrostatic forces and coordination reactions. The formation of ZnO/GO was characterized by transmission electron microscopy (TEM) and X-ray diffraction (XRD), and the antibacterial activity was investigated using a disk diffusion assay against *E. coli.* The growth curve with parameters of optical density and time indicated that the strong antibacterial activity of ZnO/GO against *E. coli* depended on the concentration of Zn ions in a synergistic effect. In addition to in vivo antibacterial studies, zinc oxide has also been used to inhibit bacterial growth or biofilm formation because bioimplants are not exempt from contamination by bacteria. Zn and its oxides exhibited one of the best antibacterial effects. This growing colony of bacteria, called a biofilm, can cause chronic conditions or diseases that are usually resistant to antibiotics [119]. Research has shown that the synergistic effect of ZnO plays a significant role in inhibiting bacterial activity in vivo [120].

Jiajun et al., 2018 investigated the antibacterial activity of Zn, Mg, and graphene oxide in vivo and in vitro. They coated GO-Mg/Zn onto a titanium surface via cathode electrophoresis deposition. Then, they studied the in vitro antibacterial properties of Ti, GO-Mg, GO-Zn, and GO-Zn Mg. First, they allowed Gram-negative bacteria to grow on the surface of Ti because most of the bioimplants are made of titanium, and the bacteria grow fully on the Ti surface. The number of bacterial colonies on the GO-Zn coating was less than that on the GO-Mg coating. Among all coatings, GO-Zn and GO-Mg showed the highest inhibition of *E. coli.* They concluded that antibacterial activity was mainly due to ROS production rather than metal ion release by the agar diffusion assay [121].

Another experimental investigation by S et al. attempted to enhance the antifouling capacity of titanium metal by coating it with GO and silane. Titanium is used in condenser tubes under seawater for fast-breeder reactors because of its superior anticorrosion properties. Despite the anticorrosive nature of titanium, microbes attach to their surfaces, which affects heat transfer and power generation. To overcome this problem, a perfluorooctyltriethoxy silane (PFOTES) along with a graphene oxide membrane is coated on titanium samples similar to condenser tubes [122]. A study was conducted to fill the gap in understanding the ecotoxic potential of graphene oxide and reduced graphene oxide in complex communities in aquatic environments by exposing a single bacterial strain to graphene oxide and reducing graphene oxide [123].

Table 1. List of GM Hybrids for Environmental Applications.

Nanocomposites	Synthesis	Particle Size	Antimicrobial Effect	Environmental Effects	Reference
Graphene oxide-Cu nanocomposite	Electrochemical deposition [123]	9.5 µm particle size	The antibacterial activity is stronger in Gram-negative bacteria than in Gram-positive bacteria.	Copper nanoparticles have gained popularity due to their unique physical and chemical properties and low cost of manufacturing.	[124]
Graphene-CuO nanocomposites	Polymerization method [125]	4.5–14.5 nm	Stable metallic copper nanoparticles (Cu-NPs) possess a significant capacity for bacterial cell filamentation and cell death.	Copper-oxide-NP-based amperometric biosensors were used to detect adenine and guanine simultaneously.	[124]
Graphene oxide-silver nanocomposites	Drop casting techniques [14]	55 nm.	The therapeutic use of silver prompted the development of the first Ag(I)-NHC compound with antibacterial characteristics.	The use of phytofunctionalized silver nanoparticles is for the suppression of microbial growth and environmental remediation.	[12]
Graphene oxide–magnetite nanocomposites	Dispersion technique [126]	10–15 nm	NCs rGO/Fe_3O_4 showed antifungal activities against Trichophyton mentagrophytes and Candida albicans by the agar-well diffusion method	A variety of applications are seen, such as catalysts, adsorbents, fuel cell batteries, supercapacitors, and wastewater treatment.	[127]

Table 2. Biomedical Applications of Graphene Oxide–Metal hybrids.

Nanocomposite	Shape	Properties	Application	Reference
GO-Cu	N/A	N/A	Carcinogenic streptococcus mutans	[128]
Graphene-Cu-zinc oxide	Nanoflowers	Biosensor	Glucose detection	[129]
Copper-beta cyclodextrin–graphene oxide	Nanoparticles	Biosensor	Tetracycline antibiotics	[130]
rGO-nickel-copper	Bimetallic hollow nanoparticles	Biosensor	Glucose detection	[131]
rGO-copper vanadate	Nanoparticles	Biosensor	Antiandrogen drug detection of nilutamide detection	[132]
Gold–copper–phosphate–graphene oxide–chicken egg white	Nanoflowers	Biosensor	Detection of acsorbic acid	[133]
Fe-Cu-rGO@Ag	Nanocomposite	Biosensor	Blood creatinine	[134]
poly-T-templated copper nanoparticles (poly T-CuNPs)-graphene oxide	Nanoparticles	Label-free fluorescent biosensor	Detection of MiRNA	[135]
GO/Cu_2O	Nanocomposite	Water treatment	Catalytic degradation rate of diclofenac (DCF)	[136]
GO/Ni	Nanocomposite	Antibacterial activity	Detection of intracellular reactive oxygen species (ROS)	[137]
(RhB/Au/RGO)	Nanocomposite	Immunosensor	Detection of Listeria monocytogenes	[138]
GO/TiO_2/blackberry extract	Partial bone nanocomposite substitutes	Tissue engineering.	Induces an osteoinductive effect	[139]

Table 3. List of Graphene Oxide–Metal Hybrids used in CO_2 Adsorption.

Material	Pressure, Bar	CO_2 Adsorption, mmol/gm	Reference
Polymerized ionic liquid/HEG	1	0.51	[140]
Spongy-graphene	1.01	0.86	[141]
MOF-AGO	1	0.54	[142]
rGO@MgO/C	1.00	0.72	[143]
B-doped rGO	1	1.8	[144]
3D PEI/GO	1	2.54	[145]
N-doped graphene aerogel	1	2.57	[146]
Nanoporous graphene	1	2.89	[147]
ZnO/N/rGO	1.01	3.55	[148]
Cu-MOF/rGO-1	1	8.19	[149]
Cu-MOF/rGO-2	1.01	8.26	[150]
Activated graphene-derived carbon	20	21.1	[151]
Graphene nanoplates	30.00	56.40	[152]
Ag@SGO	37.00	7.63	[153]
TiO_2-GO	1.00	1.88	[154]
Fe_3O_4-HEG	11.00	60.00	[155]
PANI-HEG	11.00	75.00	[156]
CuO-ZnO-ZrO_2-GO	20	209.6	[157]

Table 4. Thermodynamic parameters from the literature with adsorption of heavy metals and dyes using graphene oxide–metal hybrids.

Adsorbent	Absorbate	Temp (K)	G (kJ/mol)	Δ H (kJ/mol)	ΔS (J/mol K)	Reference
Graphene oxide	U(VI)	298	−23.54	2.98	87.02	[158]
		313	−24.88	-	-	
		340	−25.93	-	-	
Graphene oxide	Th (IV)	298	−29.91	3.59	88.32	[159]
		313	−31.45	-	-	
		338	−34.24	-	-	
Graphene oxide	Cr (VI)	298	−771.407	172.32	57.44	[160]
		303	−284.504	-	-	
		323	−968.688	-	-	
		333	−3586.05	-	-	
		343	−1198.432	-	-	
Graphene oxide	Co (II)	293	−1.035	0.588	0.005	[161]
		308	−1.105	-	-	
		323	−1.201	-	-	
Graphene oxide	Zn (II)	293.15	−37.89	−2.171	0.137	[162]
		303.15	−39.44	-	0.136	
		318.15	−40.96	-	0.134	

Table 4. *Cont.*

Adsorbent	Absorbate	Temp (K)	G (kJ/mol)	Δ H (kJ/mol)	ΔS (J/mol K)	Reference
Graphene oxide	Cs(I)	298	−23.64	10.351	110.992	[65]
		318	−25.22	-	-	
		338	−26.81	-	-	
GO-magnesium	U(VI)	303	−4.42	−1.709	8.946	[163]
		313	−4.51	-	-	
		323	−4.6	-	-	
		333	−4.69	-	-	
Sulfonated GO	U(VI)	288.15	−19.94	18.95	134.97	[164]
		293.15	−20.62	-	-	
		298.15	−21.29	-	-	
		303.15	−21.97	-	-	
		308.15	−22.64	-	-	
		313.15	−23.62	-	-	
		318.15	−23.99	-	-	
		323.15	−24.67	-	-	
		288.15	−23.68	28.56	181.28	
		293.15	−24.58	-	-	
		298.15	−25.49	-	-	
		303.15	−26.4	-	-	
		308.15	−27.3	-	-	
		313.15	−28.21	-	-	
		318.15	−29.11	-	-	
		323.15	−30.02	-	-	
GO-activated carbon felt	U (VI)	298	−20.6	10.9	105.7	[165]
		308	−21.7	-	-	
		318	−22.7	-	-	
		298	−23.3	5.7	97.2	
		308	−24.3	-	-	
		318	−25.2	-	-	
GO-CdS composite	Cu (II)	298	−14.6385	13.8079	95.631	[166]
		313	−16.2385	-	-	
		328	−17.4964	-	-	
MnO_2-GONRs	Th (IV)	293	−22.61	84.14	364.33	[58]
		298	−24.43	-	-	
		303	−26.25	-	-	
		308	−28.08	-	-	
3D-SRGO	Cd (II)	298	−6.508	19.56	87.63	[167]
		318	−8.401	-	-	
		338	−10.019	-	-	

Table 4. *Cont.*

Adsorbent	Absorbate	Temp (K)	G (kJ/mol)	Δ H (kJ/mol)	ΔS (J/mol K)	Reference
Magnetic GO nanocomposite	Mn (II), Zn (II)	283.15	−9.9598	20.8592	108.8435	[168]
		288.15	−10.504	-	-	
		293.15	−11.0483	-	-	
		298.15	−11.5925	-	-	
		303.15	−12.1367	-	-	
		308.15	−12.6809	-	-	
		283.15	−6.2028	20.9902	96.0376	
		288.15	−6.683	-	-	
		293.15	−7.1632	-	-	
		298.15	−7.6434	-	-	
		303.15	−8.1236	-	-	
		308.15	−8.6038	-	-	
(GO-f)	Cd (II), Hg (II), As (III)	298	−7.349	32.919	165.061	[169]
		308	−8.7	-	-	
		318	−10.05	-	-	
		298	−4.38	17.497	73.375	
		308	−5.114	-	-	
		318	−5.848	-	-	
		298	0.156	12.395	41.048	
		308	−0.254	-	-	
		318	−0.665	-	-	
		298	−11.914	13.268	484.981	
		308	−16.764	-	-	
		318	−21.613	-	-	
		298	−6.045	19.061	84.204	
		308	−6.887	-	-	
		318	−7.729	-	-	
		298	−1.513	11.939	45.118	
		308	−1.964	-	-	
		318	−2.416	-	-	
MnO_2–Fe_3O_4–rGO	U(VI)	298.15	−2.603	16.25	63.23	[170]
		308.15	−3.222	-	-	
		318.15	−3.872	-	-	
		328.15	−4.492	-	-	
ZnO-GO	Cr (VI)	298.15	−3.777	1.02	16.092	[171]
		303.15	−3.858	-	-	
		308.15	−3.938	-	-	
MGONRs	Th (IV)	298	−18.16	29.18	158.85	[172]
		303	−18.95	-	-	
		308	−19.74	-	-	

Table 4. *Cont.*

Adsorbent	Absorbate	Temp (K)	G (kJ/mol)	Δ H (kJ/mol)	ΔS (J/mol K)	Reference
MGO	Co (II)	293.15	−8.64	−40.87	−109.97	[173]
		298.15	−8.09	-	-	
		303.15	−7.54	-	-	
		308.15	−6.99	-	-	
		313.15	−6.44	-	-	
MGO	Hg (II), methylene blue	298	−0.29	20.8	72.3	[174]
		303	−1.26	-	-	
		313	−1.63	-	-	
		323	−2.57	-	-	
		333	−3.17	-	-	
		298	−3.38	13.4	46.8	
		303	−3.87	-	-	
		313	−4.48	-	-	
		323	−4.88	-	-	
		333	−5.61	-	-	
		298	−3.34	34.4	93.8	
		303	−3.64	-	-	
		313	−5.13	-	-	
		323	−5.29	-	-	
		333	−7.09	-	-	
		298	−4.42	27.6	63.9	
		303	−6.37	-	-	
		313	−7.85	-	-	
		323	−8.85	-	-	
		333	−10.15	-	-	
GO- Fe-Mg	Pb (II), Cu (II), Ag (II), Zn (II)	288	−19.931	14.3	118.849	[175]
		298	-	-	-	
		308	-	-	-	
		288	−13.315	25.627	134.878	
		298	-	-	-	
		308	-	-	-	
		288	−17.347	43.676	211.442	
		298	-	-	-	
		308	-	-	-	
		288	−16.481	33.471	173.023	
		298	-	-	-	
		308	-	-	-	
GO-metal organic framework	Pb (II)	293	−9.59	3.69	0.05	[176]
		303	−10.03	-	-	
		313	−10.49	-	-	

Table 4. *Cont.*

Adsorbent	Absorbate	Temp (K)	G (kJ/mol)	Δ H (kJ/mol)	ΔS (J/mol K)	Reference
GO	Eu (III)	298	−24.4503	14.5826	150.4064	[177]
		318	−27.6547	13.9978	-	
		338	−30.4665	13.8057	-	
GO	Gd (III)	303	−26.22	0.07	86.74	[178]
		323	−27.95	-	-	
		343	−29.69	-	-	
GO nanocomposite	Co (II)	298	−21.3	−10.77	35.49	[179]
		313	−21.8	-	-	
		328	−22.4	-	-	
GO–Al13	Cd (II)	298	−4.4	17.38	73.27	[179]
		308	−5.28	-	-	
		318	−5.86	-	-	
MGO	Eu (III)	293	−18.15	28.95	179.46	[180]
		313	−19.96	-	-	
		333	−21.32	-	-	
		293	−16.64	24.53	141.74	
		313	−17.53	-	-	
		333	−19.89	-	-	
GO-$MnFe_2O_4$	Pb (II), As (V), As (III)	298	−6.46	4.01	-	[181]
		313	−7.01	-	-	
		333	−7.76	-	-	
		298	−6.17	5.18	-	
		313	−6.69	-	-	
		333	−7.5	-	-	
		298	−5.7	6.13	-	
		313	−6.32	-	-	
		333	−7.09	-	-	
		298	−5.55	6.36	-	
		313	−6.14	-	-	
		333	−6.95	-	-	
		298	−5.53	6.56	-	
		313	−6.17	-	-	
		333	−6.95	-	-	
		298	−5.4	7.25	-	
		313	−6.09	-	-	
		333	−6.89	-	-	
GO-Fe_3O_4	Cr (VI)	298	−3.009	−9.174	−0.02068	[182]
		303	−2.905	-	-	
		313	−2.699	-	-	
		323	−2.492	-	-	

Table 5. List of graphene oxide–metal hybrids used in adsorption of uranium isotopes.

Material	Temperature	Gibbs Free Energy	Reference
AOMGO	298	−22.34	[59]
	318	−24.73	
	338	−27.59	
GO/SiO_2	298.15	−3.4	[60]
	298	−8.69	
	308	−9.57	[183]
$CoFe_2O_4$-rGO	318	−10.45	
	328	−11.33	
	298.15	−2.603	
MnO_2-Fe_3O_4-rGO	308.15	−3.222	[170]
	318.15	−3.872	
	328.15	−4.492	
	298	−19.58	
Cucurbit [6]uril/GO-Fe_3O_4	308	−20.76	[184]
	318	−21.93	
	328	−23.11	
	298	−8.08	
$NiCo_2O_4$@rGO	308	−8.74	[185]
	318	−9.43	
	298	−9.72	
FG−20	313	−7.05	[186]
	323	−5.6	
	333	−5.12	
	298	−9.947	
mGO-PAO	308	−12.082	[187]
	318	−14.217	
	303	−11.06	
	313	−12.13	
rGO/Fe_3O_4/TW	323	−13.2	[188]
	333	−14.26	
	303	−4.42	
	313	−4.51	
GOMO	323	−4.6	[163]
	333	−4.69	
	298	−26.71	
Fe:Ni/GO	308	−27.88	[189]
	318	−29.68	
CMC/MGOs	301	−23.31	[190]
	318	−25.29	
	338	−27.97	
	303	−8.2523	

Table 5. *Cont.*

Material	Temperature	Gibbs Free Energy	Reference
$GO/Fe_2O_3/GC$	313	−8.9065	[191]
	323	−9.5607	
	333	−10.2149	
	288.15	−5.1629	
MGO-C6	288.12	−6.4732	[192]
	298.15	−7.6856	
	303.15	−9.6564	
	308.15	−10.2449	
$GO/Fe_3O_4/GC$	303	−8.2523	[191]
	313	−8.9065	
	323	−9.5607	
	333	−10.2149	
MXene/graphene oxide	298	−399.1	[193]
	308	−474.5	
	318	−541.4	
PCN−222/GO-COOH	298.15	−8.29	[194]
	303.15	−8.55	
	308.15	−8.8	
	313.15	−9.05	
	318.15	−9.3	
	323.15	−9.55	
CS-GO-DO/ZnO	298.15	−7.18	[195]
	308.15	−8.23	
	318.15	−9.27	
	328.15	−10.31	
PdO/SiO_2@GO−1.0	298	–3.85	[196]
	303	–3.67	
	313	–3.31	
	323	–2.94	
	333	–2.58	

Table 6. List of graphene oxide–metal hybrids used in radiation shielding.

Name	Thickness (Micrometer)	Shielding Efficiency (dB)	f/GHZ	Reference
rGO	93.1	61.6	12.4	[197]
Cu/LG	8.8	63.29	18	[198]
Graphene/PMMA	33	60	-	[199]
Fe_3O_4–rGO	1	59.41	8.29	[200]
δ-MnO_2-rGO	0.3	39	8	[201]
$BaFe_{12}O_{19}$@RGO	3	32	-	[202]
Graphene film	8.4	20	8	[203]

Table 6. *Cont.*

Name	Thickness (Micrometer)	Shielding Efficiency (dB)	f/GHZ	Reference
CuS/RGO	1	64	2.3	[100]
TiO_2-Ti_3C_2TX/G	5.25	30	12.4	[204]
rGO-Al_2O_3	3	38	-	[205]
CuNWs-TAGA- GO	10	47	-	[206]
GO/Ag-7L	8	62	-	[207]
Ni/GO/PVA	2	87	-	[208]
Lignin-carbon-rGO	2	70.5	8.2–12.4	[209]
CMF/rGO/Ag	5	63.2	8.2–12.4	[210]
GO	3.2	68	8.2–12.4	[211]

Table 7. Adsorption of Methylene Blue by Graphene Oxide–Metal Hybrids.

Adsorbent	Surface Area (m^2/g)	Adsorption Capacity	Reference
$MnFe_2O_4$-rGO-MB	95	105	[212]
$MgFe_2O_4$/rGO-MB	35	24.81	[213]
GO-gC_3N_4-Fe_3O_4-MB	120	220	[214]
MHAGO-MB	-	59	[215]
PSGO-MB	229	116.7	[216]
Xanthate-Fe_3O_4-GO-MB	30.13	526.3	[217]
$NiFe_2O_4$@GO-MB	76.7	76.0	[218]
CMC/GO-MB	800.85	245	[219]
GO–MnO_2-MB	-	178.253	[220]
Alg/GO-MB	-	12.5	[221]
AC-GO-MB	-	1000	[222]
PVP/rGO/$CoFe_2O_4$-MB	240.9	333.3	[223]
CS-Fe_3O_4-GO-MB	-	261.8	[224]
Magnetic carbonate hydroxyapatite/GO	105.95	546.4	[225]

4. Other Applications and Discussion

Oil and natural dissolvable spillage mishaps are becoming more normal causing genuine ecological dangers. Although the adaptation and control of oil material are basic, oil spillage and anthropogenic outflows will undoubtedly occur here. The most common absorbent materials have drawbacks, such as environmental incompatibilities, low absorption capabilities, and poor recyclability, despite being widely used in practical applications. The selectivity and effectiveness of the separation are particularly low, because most of these materials absorb water in addition to oils. Therefore, an ideal absorbent material should have qualities such as high oil absorption capacity, high selectivity, low density, outstanding recyclability, and environmental friendliness. Consequently, strategies for the adsorption and reuse of oil and natural foreign substances should be developed.

However, in numerous environments, a combination of natural contamination and heavy metal particles exists, and their sorption affects the destiny and transport of pollutants. Communication with existing heavy metal particles may also impact the adsorption of natural toxins in graphene. This adsorption trademark should help researchers in their study of the construction and systems of adsorptive areas for graphene materials. Therefore,

understanding the coadsorption of natural impurities and heavy metal particles is essential for evaluating the ecological effects of graphene materials and planning new materials for contamination control. In the case of dye adsorption and removal, more research is needed to determine the potential applicability of graphene oxide–metal composites in real scenarios. Fume contamination is a serious issue in modern life, both at home and in the workplace. Graphene oxide–metal hybrids have shown exceptional fume recognition capacities, especially for NO_2, NO, CO, CO_2, NH_3, SO_2, H_2, and C_{l2}, and natural fumes such as $(CH_3)_2CO$, benzene, and toluene [226,227]. Graphene and GO sponges have a substantial capacity to be used with oil, diesel, gasoline, motors, and vacuum oils because of their high specific surface area, adaptable pore structure, and highly tunable surface chemistry [228].

5. Conclusions and Outlook

Blending, functionalising and using graphene nanocomposites is state of the art. All the research work paves the way for the use of graphene nanocomposites in modern applications and prepares them for advanced energy modifications and capacity enhancements. This work can provide an overview of future research in graphene-based hybrid materials.

1. While GM hybrids are making progress in a variety of environmental applications under laboratory conditions, the potential for their large-scale or real-world application has yet to be explored and tested.
2. In laboratory tests, energy configurations made from graphene nanocomposites have already shown good results. To develop high-end devices that work on a large scale, it is necessary to produce a large number of excellent graphene nanocomposites, whose electrical and chemical properties must of course remain stable throughout the operation.
3. In the face of increasing water pollution from industrial waste, graphene nanocomposites are particularly attractive because they selectively degrade pollutants by light, even in the presence of natural and foreign substances. It is still too early to expect the widespread application of these nanocomposites for environmental monitoring and remediation, as important questions about the short- and long-term effects of graphene on biological systems and humans remain largely unanswered.
4. Currently, large-scale applications of graphene-based achievements are possible in electrochemical energy storage and simple compounds in photovoltaics and optoelectronics. With the development of key physical sciences as well as down-to-earth methods, there will be further advanced applications due to graphene and graphene nanocomposites.

Author Contributions: Conceptualization—G.L.; Writing—Original draft preparation, E.F.J.; Writing—review and editing, G.L.; Visualization—E.F.J.; Supervision—G.L. All authors have read and agreed to the published version of the manuscript.

Funding: This research received no external funding.

Data Availability Statement: Not applicable.

Conflicts of Interest: The authors declare no conflict of interest.

References

1. Bijesh, P.; Selvaraj, V.; Andal, V. A review on synthesis and applications of nano metal Oxide/porous carbon composite. *Mater. Today Proc.* **2021**, *55*, 212–219. [CrossRef]
2. Li, F.; Jiang, X.; Zhao, J.; Zhang, S. Graphene oxide: A promising nanomaterial for energy and environmental applications. *Nano Energy* **2015**, *16*, 488–515. [CrossRef]
3. Bandosz, T.J.; Petit, C. MOF/graphite oxide hybrid materials: Exploring the new concept of adsorbents and catalysts. *Adsorption* **2010**, *17*, 5–16. [CrossRef]
4. Zhang, X.; Guo, Y.X.; Ren, B.; Zhao, N.; Hu, Y.C.; Wang, X. Preparation of graphene oxide membranes by vacuum self-assembly for copper separation in water. *Diam. Relat. Mater.* **2021**, *120*, 108687. [CrossRef]

5. Wang, Q.; Wang, B.-T. Surface plasmon resonance biosensor based on graphene oxide/silver coated polymer cladding silica fiber. *Sens. Actuators B Chem.* **2018**, *275*, 332–338. [CrossRef]
6. Chanda, D.; Hnát, J.; Dobrota, A.S.; Pašti, I.A.; Paidar, M.; Bouzek, K. The effect of surface modification by reduced graphene oxide on the electrocatalytic activity of nickel towards the hydrogen evolution reaction. *Phys. Chem. Chem. Phys.* **2015**, *17*, 26864–26874. [CrossRef]
7. Zhu, C.; Han, L.; Hu, P.; Dong, S. In situ loading of well-dispersed gold nanoparticles on two-dimensional graphene oxide/SiO2 composite nanosheets and their catalytic properties. *Nanoscale* **2012**, *4*, 1641–1646. [CrossRef] [PubMed]
8. Chen, X.; Wu, G.; Chen, J.; Chen, X.; Xie, Z.; Wang, X. Synthesis of "Clean" and Well-Dispersive Pd Nanoparticles with Excellent Electrocatalytic Property on Graphene Oxide. *J. Am. Chem. Soc.* **2011**, *133*, 3693–3695. [CrossRef]
9. Ogata, C.; Koinuma, M.; Hatakeyama, K.; Tateishi, H.; Asrori, M.Z.; Taniguchi, T.; Funatsu, A.; Matsumoto, Y. Metal Permeation into Multi-layered Graphene Oxide. *Sci. Rep.* **2014**, *4*, 3647. [CrossRef]
10. Chan, K.T.; Neaton, J.B.; Cohen, M.L. First-principles study of metal adatom adsorption on graphene. *Phys. Rev. B* **2008**, *77*, 235430. [CrossRef]
11. Bu, I.Y.; Huang, R. Fabrication of CuO-decorated reduced graphene oxide nanosheets for supercapacitor applications. *Ceram. Int.* **2017**, *43*, 45–50. [CrossRef]
12. Yadav, S.; Jain, A.; Malhotra, P. A review on the sustainable routes for the synthesis and applications of cuprous oxide nanoparticles and their nanocomposites. *Green Chem.* **2019**, *21*, 937–955. [CrossRef]
13. Chen, Q.; Zhang, L.; Chen, G. Facile Preparation of Graphene-Copper Nanoparticle Composite by in Situ Chemical Reduction for Electrochemical Sensing of Carbohydrates. *Anal. Chem.* **2011**, *84*, 171–178. [CrossRef]
14. Neto, S.M.; Almeida, K.C.D.; Macedo, M.L.R.; Franco, O.L. Understanding bacterial resistance to antimicrobial peptides: From the surface to deep inside. *Biochim. Biophys. Acta (BBA) -Mol. Cell Res.* **2015**, *1848 Pt B*, 3078–3088. [CrossRef]
15. Carolin, C.F.; Kumar, P.S.; Saravanan, A.; Joshiba, G.J.; Naushad, M. Efficient techniques for the removal of toxic heavy metals from aquatic environment: A review. *J. Environ. Chem. Eng.* **2017**, *5*, 2782–2799. [CrossRef]
16. Wang, B.; Zhang, F.; He, S.; Huang, F.; Peng, Z. Adsorption Behaviour of Reduced Graphene Oxide for Removal of Heavy Metal Ions. *Asian J. Chem.* **2014**, *26*, 4901–4906. [CrossRef]
17. Su, H.; Ye, Z.; Hmidi, N. High-performance iron oxide–graphene oxide nanocomposite adsorbents for arsenic removal. *Colloids Surf. A Physicochem. Eng. Asp.* **2017**, *522*, 161–172. [CrossRef]
18. Fathy, M.; Moghny, T.A.; Mousa, M.A.; Abdou, M.M.; El-Bellihi, A.-H.A.-A.; Awadallah, A.E. Correction to: Absorption of calcium ions on oxidized graphene sheets and study its dynamic behavior by kinetic and isothermal models. *Appl. Nanosci.* **2018**, *8*, 2105. [CrossRef]
19. Wang, J.; Chen, B. Adsorption and coadsorption of organic pollutants and a heavy metal by graphene oxide and reduced graphene materials. *Chem. Eng. J.* **2015**, *281*, 379–388. [CrossRef]
20. Huang, H.; Wang, Y.; Zhang, Y.; Niu, Z.; Li, X. Amino-functionalized graphene oxide for Cr(VI), Cu(II), Pb(II) and Cd(II) removal from industrial wastewater. *Open Chem.* **2020**, *18*, 97–107. [CrossRef]
21. Wan, S.; He, F.; Wu, J.; Wan, W.; Gu, Y.; Gao, B. Rapid and highly selective removal of lead from water using graphene oxide-hydrated manganese oxide nanocomposites. *J. Hazard. Mater.* **2016**, *314*, 32–40. [CrossRef] [PubMed]
22. Naeem, H.; Ajmal, M.; Qureshi, R.B.; Muntha, S.T.; Farooq, M.; Siddiq, M. Facile synthesis of graphene oxide–silver nanocomposite for decontamination of water from multiple pollutants by adsorption, catalysis and antibacterial activity. *J. Environ. Manag.* **2018**, *230*, 199–211. [CrossRef]
23. Lotfi, Z.; Mousavi, H.Z.; Sajjadi, S.M. Covalently bonded double-charged ionic liquid on magnetic graphene oxide as a novel, efficient, magnetically separable and reusable sorbent for extraction of heavy metals from medicine capsules. *RSC Adv.* **2016**, *6*, 90360–90370. [CrossRef]
24. Dong, Y.; Wang, L.; Wang, J.; Wang, S.; Wang, Y.; Jin, D.; Chen, P.; Du, W.; Zhang, L.; Liu, B.-F. Graphene-Based Helical Micromotors Constructed by "Microscale Liquid Rope-Coil Effect" with Microfluidics. *ACS Nano* **2020**, *14*, 16600–16613. [CrossRef]
25. Peng, W.; Li, H.; Liu, Y.; Song, S. A review on heavy metal ions adsorption from water by graphene oxide and its composites. *J. Mol. Liq.* **2017**, *230*, 496–504. [CrossRef]
26. Archana, S.; Jayanna, B.; Ananda, A.; Shilpa, B.M.; Pandiarajan, D.; Muralidhara, H.; Kumar, K.Y. Synthesis of nickel oxide grafted graphene oxide nanocomposites—A systematic research on chemisorption of heavy metal ions and its antibacterial activity. *Environ. Nanotechnol. Monit. Manag.* **2021**, *16*, 100486. [CrossRef]
27. Fu, Y.; Wang, J.; Liu, Q.; Zeng, H. Water-dispersible magnetic nanoparticle–graphene oxide composites for selenium removal. *Carbon* **2014**, *77*, 710–721. [CrossRef]
28. Zito, C.A.; Perfecto, T.M.; Mazon, T.; Dippel, A.-C.; Koziej, D.; Volanti, D.P. Reoxidation of graphene oxide: Impact on the structure, chemical composition, morphology and dye adsorption properties. *Appl. Surf. Sci.* **2021**, *567*, 150774. [CrossRef]
29. Al-Degs, Y.; El-Barghouthi, M.; El-Sheikh, A.; Walker, G. Effect of solution pH, ionic strength, and temperature on adsorption behavior of reactive dyes on activated carbon. *Dye. Pigment.* **2008**, *77*, 16–23. [CrossRef]
30. Sharma, P.; Das, M.R. Removal of a Cationic Dye from Aqueous Solution Using Graphene Oxide Nanosheets: Investigation of Adsorption Parameters. *J. Chem. Eng. Data* **2012**, *58*, 151–158. [CrossRef]
31. Zang, H.; Li, Y.; Li, Y.; Chen, L.; Du, Q.; Zhou, K.; Li, H.; Wang, Y.; Ci, L. Adsorptive Removal of Cationic Dye from Aqueous Solution by Graphene Oxide/Cellulose Acetate Composite. *J. Nanosci. Nanotechnol.* **2019**, *19*, 4535–4542. [CrossRef] [PubMed]

32. Naeem, H.; Ajmal, M.; Muntha, S.; Ambreen, J.; Siddiq, M. Synthesis and characterization of graphene oxide sheets integrated with gold nanoparticles and their applications to adsorptive removal and catalytic reduction of water contaminants. *RSC Adv.* **2018**, *8*, 3599–3610. [CrossRef]
33. Zhang, J.; Gong, J.-L.; Zenga, G.-M.; Ou, X.-M.; Jiang, Y.; Chang, Y.-N.; Guo, M.; Zhang, C.; Liu, H.-Y. Simultaneous removal of humic acid/fulvic acid and lead from landfill leachate using magnetic graphene oxide. *Appl. Surf. Sci.* **2016**, *370*, 335–350. [CrossRef]
34. Yang, J.; Shojaei, S.; Shojaei, S. Removal of drug and dye from aqueous solutions by graphene oxide: Adsorption studies and chemometrics methods. *npj Clean Water* **2022**, *5*, 5. [CrossRef]
35. Pervez, N.; He, W.; Zarra, T.; Naddeo, V.; Zhao, Y. New Sustainable Approach for the Production of Fe_3O_4/Graphene Oxide-Activated Persulfate System for Dye Removal in Real Wastewater. *Water* **2020**, *12*, 733. [CrossRef]
36. Boruah, P.K.; Borah, D.J.; Handique, J.; Sharma, P.; Sengupta, P.; Das, M.R. Facile synthesis and characterization of Fe_3O_4 nanopowder and Fe_3O_4/reduced graphene oxide nanocomposite for methyl blue adsorption: A comparative study. *J. Environ. Chem. Eng.* **2015**, *3*, 1974–1985. [CrossRef]
37. Hao, Y.; Wang, Z.; Gou, J.; Dong, S. Highly efficient adsorption and removal of Chrysoidine Y from aqueous solution by magnetic graphene oxide nanocomposite. *Arab. J. Chem.* **2019**, *12*, 3064–3074. [CrossRef]
38. Al-Sabahi, J.; Bora, T.; Al-Abri, M.; Dutta, J. Efficient visible light photocatalysis of benzene, toluene, ethylbenzene and xylene (BTEX) in aqueous solutions using supported zinc oxide nanorods. *PLoS ONE* **2017**, *12*, e0189276. [CrossRef]
39. Garg, A.; Singhania, T.; Singh, A.; Sharma, S.; Rani, S.; Neogy, A.; Yadav, S.R.; Sangal, V.K.; Garg, N. Photocatalytic Degradation of Bisphenol-A using N, Co Codoped TiO_2 Catalyst under Solar Light. *Sci. Rep.* **2019**, *9*, 765. [CrossRef]
40. Xin, L.; Wu, X.; Xiang, Y.; Zhang, S.; Huang, X.; Liu, H. Binary Dye Removal from Simulated Wastewater Using Reduced Graphene Oxide Loaded with Fe-Cu Bimetallic Nanocomposites Combined with an Artificial Neural Network. *Materials* **2021**, *14*, 5268. [CrossRef]
41. Chandra, L.; Jagadish, K.; Karthikeyarajan, V.; Jalalah, M.; Alsaiari, M.; Harraz, F.A.; Balakrishna, R.G. Nitrogenated Graphene Oxide-Decorated Metal Sulfides for Better Antifouling and Dye Removal. *ACS Omega* **2022**, *7*, 9674–9683. [CrossRef] [PubMed]
42. Kanani, M.; Kanani, N.; Batooie, N.; Bozorgian, A.; Barghi, A.; Rezania, S. Removal of Rhodamine 6G dye using one-pot synthesis of magnetic manganese graphene oxide: Optimization by response surface methodology. *Environ. Nanotechnol. Monit. Manag.* **2022**, *18*, 100709. [CrossRef]
43. Ahmed, G.; Hanif, M.; Khan, A.J.; Zhao, L.; Zhang, J.; Liu, Z. ZnO flowers and graphene oxide hybridization for efficient photocatalytic degradation of o-xylene in water. *Mater. Chem. Phys.* **2018**, *212*, 479–489. [CrossRef]
44. Shen, J.-H.; Li, M.-M.; Chu, L.-F.; Guo, C.-X.; Guo, Y.-J. Effect mechanism of copper ions on photocatalytic activity of TiO2/graphene oxide composites for phenol-4-sulfonic acid photodegradation. *J. Colloid Interface Sci.* **2020**, *586*, 563–575. [CrossRef] [PubMed]
45. Yang, S.; Li, L.; Pei, Z.; Li, C.; Lv, J.; Xie, J.; Wen, B.; Zhang, S. Adsorption kinetics, isotherms and thermodynamics of Cr(III) on graphene oxide. *Colloids Surf. A Physicochem. Eng. Asp.* **2014**, *457*, 100–106. [CrossRef]
46. Sun, Y.; Wang, Q.; Chen, C.; Tan, X.; Wang, X. Interaction between Eu(III) and Graphene Oxide Nanosheets Investigated by Batch and Extended X-ray Absorption Fine Structure Spectroscopy and by Modeling Techniques. *Environ. Sci. Technol.* **2012**, *46*, 6020–6027. [CrossRef] [PubMed]
47. Mohanty, B.N.; Yuvaraj, R.; Jena, H.; Ponraju, D. Graphene Oxide as an Adsorbent for Ruthenium from Aqueous Solution. *ChemistrySelect* **2022**, *7*, e202200078. [CrossRef]
48. Erhayem, M.; Hosouna, B.; Zidan, M. Modeling and Simulation of Sorption of Pb(II) Ions onto Synthesized Graphene Oxide Surface. *J. Nanosci. Nanotechnol. Appl.* **2017**, *3*, 301. [CrossRef]
49. Kuzenkova, A.S.; Romanchuk, A.Y.; Trigub, A.L.; Maslakov, K.I.; Egorov, A.V.; Amidani, L.; Kittrell, C.; Kvashnina, K.O.; Tour, J.M.; Talyzin, A.V.; et al. New insights into the mechanism of graphene oxide and radionuclide interaction. *Carbon* **2019**, *158*, 291–302. [CrossRef]
50. Boulanger, N.; Kuzenkova, A.S.; Iakunkov, A.; Romanchuk, A.Y.; Trigub, A.L.; Egorov, A.V.; Bauters, S.; Amidani, L.; Retegan, M.; Kvashnina, K.O.; et al. Enhanced sorption of radionuclides by defect-rich graphene oxide. *ACS Appl. Mater. Interfaces* **2020**, *12*, 45122–45135. [CrossRef] [PubMed]
51. Boulanger, N.; Kuzenkova, A.S.; Iakunkov, A.; Nordenström, A.; Romanchuk, A.Y.; Trigub, A.L.; Zasimov, P.V.; Prodana, M.; Enachescu, M.; Bauters, S.; et al. High Surface Area "3D Graphene Oxide" for Enhanced Sorption of Radionuclides (Adv. Mater. Interfaces 18/2022). *Adv. Mater. Interfaces* **2022**, *9*, 2270099. [CrossRef]
52. Minitha, C.R.; Suresh, R.; Maity, U.K.; Haldorai, Y.; Subramaniam, V.; Manoravi, P.; Joseph, M.; Kumar, R.T.R. Magnetite Nanoparticle Decorated Reduced Graphene Oxide Composite as an Efficient and Recoverable Adsorbent for the Removal of Cesium and Strontium Ions. *Ind. Eng. Chem. Res.* **2018**, *57*, 1225–1232. [CrossRef]
53. Lujanienė, G.; Šemčuk, S.; Lečinskytė, A.; Kulakauskaitė, I.; Mažeika, K.; Valiulis, D.; Pakštas, V.; Skapas, M.; Tumėnas, S. Magnetic graphene oxide based nano-composites for removal of radionuclides and metals from contaminated solutions. *J. Environ. Radioact.* **2017**, *166*, 166–174. [CrossRef] [PubMed]
54. Lujanienė, G.; Šemčuk, S.; Kulakauskaitė, I.; Mažeika, K.; Valiulis, D.; Juškėnas, R.; Tautkus, S. Sorption of radionuclides and metals to graphene oxide and magnetic graphene oxide. *J. Radioanal. Nucl. Chem. Artic.* **2015**, *307*, 2267–2275. [CrossRef]

55. Wang, K.; Yan, Z.; Fu, L.; Li, D.; Gong, L.; Wang, Y.; Xiong, Y. Gemini ionic liquid modified nacre-like reduced graphene oxide click membranes for ReO_4^-/TcO_4^- removal. *Sep. Purif. Technol.* **2022**, *302*, 122073. [CrossRef]
56. Wu, X.; Yang, Q.; Xu, D.; Zhong, Y.; Luo, K.; Li, X.; Chen, H.; Zeng, G. Simultaneous Adsorption/Reduction of Bromate by Nanoscale Zerovalent Iron Supported on Modified Activated Carbon. *Ind. Eng. Chem. Res.* **2013**, *52*, 12574–12581. [CrossRef]
57. Romanchuk, A.Y.; Slesarev, A.S.; Kalmykov, S.N.; Kosynkin, D.V.; Tour, J.M. Graphene oxide for effective radionuclide removal. *Phys. Chem. Chem. Phys.* **2012**, *15*, 2321–2327. [CrossRef] [PubMed]
58. Xiu, T.; Liu, Z.; Wang, Y.; Wu, P.; Du, Y.; Cai, Z. Thorium adsorption on graphene oxide nanoribbons/manganese dioxide composite material. *J. Radioanal. Nucl. Chem. Artic.* **2019**, *319*, 1059–1067. [CrossRef]
59. Zhao, Y.; Li, J.; Zhang, S.; Chen, H.; Shao, D. Efficient enrichment of uranium(vi) on amidoximated magnetite/graphene oxide composites. *RSC Adv.* **2013**, *3*, 18952–18959. [CrossRef]
60. Meng, H.; Li, Z.; Ma, F.; Wang, X.; Zhou, W.; Zhang, L. Synthesis and characterization of surface ion-imprinted polymer based on SiO_2-coated graphene oxide for selective adsorption of uranium(vi). *RSC Adv.* **2015**, *5*, 67662–67668. [CrossRef]
61. El-Shazly, E.A.A.; Moussa, S.I.; Dakroury, G.A. Recovery of Some Rare-Earth Elements by Sorption Technique onto Graphene Oxide. *J. Sustain. Met.* **2022**, *8*, 715–731. [CrossRef]
62. Aytas, S.; Yusan, S.; Sert, S.; Gok, C. Preparation and characterization of magnetic graphene oxide nanocomposite (GO-Fe_3O_4) for removal of strontium and cesium from aqueous solutions. *Charact. Appl. Nanomater.* **2021**, *4*, 26–39. [CrossRef]
63. Xia, T.; Qi, Y.; Liu, J.; Qi, Z.; Chen, W.; Wiesner, M.R. Cation-Inhibited Transport of Graphene Oxide Nanomaterials in Saturated Porous Media: The Hofmeister Effects. *Environ. Sci. Technol.* **2017**, *51*, 828–837. [CrossRef] [PubMed]
64. Zong, P.; Wang, S.; Zhao, Y.; Wang, H.; Pan, H.; He, C. Synthesis and application of magnetic graphene/iron oxides composite for the removal of U(VI) from aqueous solutions. *Chem. Eng. J.* **2013**, *220*, 45–52. [CrossRef]
65. Tan, L.; Wang, S.; Du, W.; Hu, T. Effect of water chemistries on adsorption of Cs(I) onto graphene oxide investigated by batch and modeling techniques. *Chem. Eng. J.* **2016**, *292*, 92–97. [CrossRef]
66. Liu, X.; Gong, W.; Luo, J.; Zou, C.; Yang, Y.; Yang, S. Selective adsorption of cationic dyes from aqueous solution by polyoxometalate-based metal–organic framework composite. *Appl. Surf. Sci.* **2016**, *362*, 517–524. [CrossRef]
67. Dong, Y.; Dong, Z.; Zhang, Z.; Liu, Y.; Cheng, W.; Miao, H.; He, X.; Xu, Y. POM Constructed from Super-Sodalite Cage with Extra-Large 24-Membered Channels: Effective Sorbent for Uranium Adsorption. *ACS Appl. Mater. Interfaces* **2017**, *9*, 22088–22092. [CrossRef]
68. Nugroho, B.S.; Kato, A.; Kowa, C.; Nakashima, T.; Wada, A.; Wihadi, M.N.K.; Nakashima, S. Exploration of the Cs Trapping Phenomenon by Combining Graphene Oxide with α-$K_6P_2W_{18}O_{62}$ as Nanocomposite. *Materials* **2021**, *14*, 5577. [CrossRef]
69. Kawahara, R.; Uchida, S.; Mizuno, N. Redox-Induced Reversible Uptake–Release of Cations in Porous Ionic Crystals Based on Polyoxometalate: Cooperative Migration of Electrons with Alkali Metal Ions. *Chem. Mater.* **2015**, *27*, 2092–2099. [CrossRef]
70. Seino, S.; Kawahara, R.; Ogasawara, Y.; Mizuno, N.; Uchida, S. Reduction-Induced Highly Selective Uptake of Cesium Ions by an Ionic Crystal Based on Silicododecamolybdate. *Angew. Chem.* **2016**, *128*, 4055–4059. [CrossRef]
71. Zhang, Q.; Gao, Y.; Xu, Z.; Wang, S.; Kobayashi, H.; Wang, J. The Effects of Oxygen Functional Groups on Graphene Oxide on the Efficient Adsorption of Radioactive Iodine. *Materials* **2020**, *13*, 5770. [CrossRef]
72. Razab, M.K.A.A.; Nawi, N.M.; Hadzuan, F.H.M.; Abdullah, N.H.; Muhamad, M.; Sunaiwi, R.; Ibrahim, F.; Zin, F.A.M.; Noor, A.M. Fluorine-18 Fluorodeoxyglucose Isolation Using Graphene Oxide for Alternative Radiopharmaceutical Spillage Decontamination in PET Scan. *Sustainability* **2022**, *14*, 4492. [CrossRef]
73. Liu, Z.; Wang, Y.; Zhang, G.; Yang, J.; Liu, S. Preparation of graphene-based catalysts and combined DBD reactor for VOC degradation. *Environ. Sci. Pollut. Res.* **2022**, *29*, 51717–51731. [CrossRef]
74. Yu, L.; Wang, L.; Xu, W.; Chen, L.; Fu, M.; Wu, J.; Ye, D. Adsorption of VOCs on reduced graphene oxide. *J. Environ. Sci.* **2018**, *67*, 171–178. [CrossRef]
75. Shrivastava, S.; Thomas, S.; Sobhan, C.; Peterson, G. An experimental investigation of the CO_2 adsorption performance of graphene oxide forms. *Int. J. Refrig.* **2018**, *96*, 179–190. [CrossRef]
76. Vijay, S.; Ju, W.; Brückner, S.; Tsang, S.-C.; Strasser, P.; Chan, K. Unified mechanistic understanding of CO_2 reduction to CO on transition metal and single atom catalysts. *Nat. Catal.* **2021**, *4*, 1024–1031. [CrossRef]
77. Alves, D.C.B.; Silva, R.; Voiry, D.; Asefa, T.; Chhowalla, M. Copper nanoparticles stabilized by reduced graphene oxide for CO_2 reduction reaction. *Mater. Renew. Sustain. Energy* **2015**, *4*, 2. [CrossRef]
78. Xu, D.; Cheng, B.; Wang, W.; Jiang, C.; Yu, J. Ag_2CrO_4/g-C_3N_4/graphene oxide ternary nanocomposite Z-scheme photocatalyst with enhanced CO_2 reduction activity. *Appl. Catal. B Environ.* **2018**, *231*, 368–380. [CrossRef]
79. Habisreutinger, S.N.; Schmidt-Mende, L.; Stolarczyk, J.K. Photocatalytic Reduction of CO_2 on TiO_2 and Other Semiconductors. *Angew. Chem. Int. Ed.* **2013**, *52*, 7372–7408. [CrossRef] [PubMed]
80. Rambabu, Y.; Kumar, U.; Singhal, N.; Kaushal, M.; Jaiswal, M.; Jain, S.L.; Roy, S.C. Photocatalytic reduction of carbon dioxide using graphene oxide wrapped TiO_2 nanotubes. *Appl. Surf. Sci.* **2019**, *485*, 48–55. [CrossRef]
81. Shown, I.; Hsu, H.-C.; Chang, Y.-C.; Lin, C.-H.; Roy, P.K.; Ganguly, A.; Wang, C.-H.; Chang, J.-K.; Wu, C.-I.; Chen, L.-C.; et al. Highly Efficient Visible Light Photocatalytic Reduction of CO_2 to Hydrocarbon Fuels by Cu-Nanoparticle Decorated Graphene Oxide. *Nano Lett.* **2014**, *14*, 6097–6103. [CrossRef] [PubMed]

82. Zhu, Z.; Han, Y.; Chen, C.; Ding, Z.; Long, J.; Hou, Y. Reduced Graphene Oxide-Cadmium Sulfide Nanorods Decorated with Silver Nanoparticles for Efficient Photocatalytic Reduction Carbon Dioxide Under Visible Light. *ChemCatChem* **2018**, *10*, 1627–1634. [CrossRef]
83. Deerattrakul, V.; Dittanet, P.; Sawangphruk, M.; Kongkachuichay, P. CO_2 hydrogenation to methanol using Cu-Zn catalyst supported on reduced graphene oxide nanosheets. *J. CO2 Util.* **2016**, *16*, 104–113. [CrossRef]
84. Yue, T.; Huang, H.; Chang, Y.; Jia, J.; Jia, M. Controlled assembly of nitrogen-doped iron carbide nanoparticles on reduced graphene oxide for electrochemical reduction of carbon dioxide to syngas. *J. Colloid Interface Sci.* **2021**, *601*, 877–885. [CrossRef] [PubMed]
85. Zhang, Z.; Ahmad, F.; Zhao, W.; Yan, W.; Zhang, W.; Huang, H.; Ma, C.; Zeng, J. Enhanced Electrocatalytic Reduction of CO_2 via Chemical Coupling between Indium Oxide and Reduced Graphene Oxide. *Nano Lett.* **2019**, *19*, 4029–4034. [CrossRef] [PubMed]
86. Saquib, M.; Halder, A. Reduced graphene oxide supported gold nanoparticles for electrocatalytic reduction of carbon dioxide. *J. Nanopart. Res.* **2018**, *20*, 46. [CrossRef]
87. Wu, D.; Chen, W.; Wang, X.; Fu, X.-Z.; Luo, J.-L. Metal-support interaction enhanced electrochemical reduction of CO_2 to formate between graphene and Bi nanoparticles. *J. CO2 Util.* **2020**, *37*, 353–359. [CrossRef]
88. Cheng, J.; Zhang, M.; Wu, G.; Wang, X.; Zhou, J.; Cen, K. Photoelectrocatalytic Reduction of CO_2 into Chemicals Using Pt-Modified Reduced Graphene Oxide Combined with Pt-Modified TiO_2 Nanotubes. *Environ. Sci. Technol.* **2014**, *48*, 7076–7084. [CrossRef] [PubMed]
89. Kumar, P.; Mungse, H.P.; Khatri, O.P.; Jain, S.L. Nitrogen-doped graphene-supported copper complex: A novel photocatalyst for CO_2 reduction under visible light irradiation. *RSC Adv.* **2015**, *5*, 54929–54935. [CrossRef]
90. Shang, S.; Tao, Z.; Yang, C.; Hanif, A.; Li, L.; Tsang, D.C.; Gu, Q.; Shang, J. Facile synthesis of CuBTC and its graphene oxide composites as efficient adsorbents for CO_2 capture. *Chem. Eng. J.* **2020**, *393*, 124666. [CrossRef]
91. Altass, H.M.; Morad, M.; Khder, A.E.-R.S.; Mannaa, M.A.; Jassas, R.S.; Alsimaree, A.A.; Ahmed, S.A.; Salama, R.S. Enhanced Catalytic Activity for CO Oxidation by Highly Active Pd Nanoparticles Supported on Reduced Graphene Oxide /Copper Metal Organic Framework. *J. Taiwan Inst. Chem. Eng.* **2021**, *128*, 194–208. [CrossRef]
92. Gunathilake, C.A.; Ranathunge, G.G.T.A.; Dassanayake, R.S.; Illesinghe, S.D.; Manchanda, A.S.; Kalpage, C.S.; Rajapakse, R.M.G.; Karunaratne, D.G.G.P. Emerging investigator series: Synthesis of magnesium oxide nanoparticles fabricated on a graphene oxide nanocomposite for CO_2 sequestration at elevated temperatures. *Environ. Sci. Nano* **2020**, *7*, 1225–1239. [CrossRef]
93. Minitha, C.R.; Anithaa, V.S.; Subramaniam, V.; Kumar, R.T.R. Impact of Oxygen Functional Groups on Reduced Graphene Oxide-Based Sensors for Ammonia and Toluene Detection at Room Temperature. *ACS Omega* **2018**, *3*, 4105–4112. [CrossRef] [PubMed]
94. Lim, S.T.; Kim, J.H.; Lee, C.Y.; Koo, S.; Jerng, D.-W.; Wongwises, S.; Ahn, H.S. Mesoporous graphene adsorbents for the removal of toluene and xylene at various concentrations and its reusability. *Sci. Rep.* **2019**, *9*, 10922. [CrossRef]
95. Faghihi-Zarandi, A.; Rakhtshah, J.; Yarahmadi, B.B.; Shirkhanloo, H. A rapid removal of xylene vapor from environmental air based on bismuth oxide coupled to heterogeneous graphene/ graphene oxide by UV photo-catalectic degradation-adsorption procedure. *J. Environ. Chem. Eng.* **2020**, *8*, 104193. [CrossRef]
96. Mateo, D.; Albero, J.; García, H. Graphene supported NiO/Ni nanoparticles as efficient photocatalyst for gas phase CO_2 reduction with hydrogen. *Appl. Catal. B Environ.* **2018**, *224*, 563–571. [CrossRef]
97. Xi, J.; Li, Y.; Zhou, E.; Liu, Y.; Gao, W.; Guo, Y.; Ying, J.; Chen, Z.; Chen, G.; Gao, C. Graphene aerogel films with expansion enhancement effect of high-performance electromagnetic interference shielding. *Carbon* **2018**, *135*, 44–51. [CrossRef]
98. Xu, L.; Zhang, W.; Wang, L.; Xue, J.; Hou, S. Large-scale preparation of graphene oxide film and its application for electromagnetic interference shielding. *RSC Adv.* **2021**, *11*, 33302–33308. [CrossRef] [PubMed]
99. Shi, K.; Su, J.; Liang, H.; Hu, K.; Xu, J. Highly optically transparent graphene mesh for electromagnetic interference shielding. *Diam. Relat. Mater.* **2022**, *123*, 108849. [CrossRef]
100. Ghosh, K.; Srivastava, S.K. Enhanced Supercapacitor Performance and Electromagnetic Interference Shielding Effectiveness of CuS Quantum Dots Grown on Reduced Graphene Oxide Sheets. *ACS Omega* **2021**, *6*, 4582–4596. [CrossRef] [PubMed]
101. Li, J.; Huang, L.; Yuan, Y.; Li, Y.; He, X. Mechanically strong, thermally conductive and flexible graphene composite paper for exceptional electromagnetic interference shielding. *Mater. Sci. Eng. B* **2020**, *263*, 114893. [CrossRef]
102. Kumar, P.; Shahzad, F.; Hong, S.M.; Koo, C.M. A flexible sandwich graphene/silver nanowires/graphene thin film for high-performance electromagnetic interference shielding. *RSC Adv.* **2016**, *6*, 101283–101287. [CrossRef]
103. Fu, P.; Huan, X.; Luo, J.; Ren, S.; Jia, X.; Yang, X. Magnetically Aligned Fe_3O_4 Nanowires-Reduced Graphene Oxide for Gas Barrier, Microwave Absorption, and EMI Shielding. *ACS Appl. Nano Mater.* **2020**, *3*, 9340–9355. [CrossRef]
104. Qu, Z.; Wang, Y.; Wang, W.; Yu, D. Robust magnetic and electromagnetic wave absorption performance of reduced graphene oxide loaded magnetic metal nanoparticle composites. *Adv. Powder Technol.* **2020**, *32*, 194–203. [CrossRef]
105. Torrisi, L.; Silipigni, L.; Cutroneo, M. Graphene oxide as a radiation sensitive material for XPS dosimetry. *Vacuum* **2020**, *173*, 109175. [CrossRef]
106. Silipigni, L.; Cutroneo, M.; Salvato, G.; Torrisi, L. In-situ soft X-ray effects on graphene oxide films. *Radiat. Eff. Defects Solids* **2018**, *173*, 740–750. [CrossRef]

107. Malinský, P.; Macková, A.; Florianová, M.; Cutroneo, M.; Hnatowicz, V.; Boháčová, M.; Szőkölová, K.; Böttger, R.; Sofer, Z. The Structural and Compositional Changes of Graphene Oxide Induced by Irradiation With 500 keV Helium and Gallium Ions. *Phys. Status Solidi (b)* **2018**, *256*, 1800409. [CrossRef]
108. Malinský, P.; Cutroneo, M.; Sofer, Z.; Szőkölová, K.; Böttger, R.; Akhmadaliev, S.; Macková, A. Structural and compositional modification of graphene oxide by means of medium and heavy ion implantation. *Nucl. Instrum. Methods Phys. Res. Sect. B Beam Interact. Mater. At.* **2019**, *460*, 201–208. [CrossRef]
109. Kumar, P.; Shahzad, F.; Yu, S.; Hong, S.M.; Kim, Y.-H.; Koo, C.M. Large-area reduced graphene oxide thin film with excellent thermal conductivity and electromagnetic interference shielding effectiveness. *Carbon* **2015**, *94*, 494–500. [CrossRef]
110. Hosseini, S.H.; Askari, M.; Ezzati, S.N. X-ray attenuating nanocomposite based on polyaniline using Pb nanoparticles. *Synth. Met.* **2014**, *196*, 68–75. [CrossRef]
111. Zarei, M.; Sina, S.; Hashemi, S.A. Superior X-ray radiation shielding of biocompatible platform based on reinforced polyaniline by decorated graphene oxide with interconnected tungsten–bismuth–tin complex. *Radiat. Phys. Chem.* **2021**, *188*, 109588. [CrossRef]
112. Kwon, D.-J.; Kwon, I.-J.; Milam-Guerrero, J.; Yang, S.B.; Yeum, J.H.; Choi, H.H. Aramid nanofiber-reinforced multilayer electromagnetic-interference (EMI) shielding composites with high interfacial durability. *Mater. Des.* **2022**, *215*, 110452. [CrossRef]
113. Xie, F.; Gao, K.; Zhuo, L.; Jia, F.; Ma, Q.; Lu, Z. Robust Ti3C2Tx/RGO/ANFs hybrid aerogel with outstanding electromagnetic shielding performance and compression resilience. *Compos. Part A Appl. Sci. Manuf.* **2022**, *160*, 107049. [CrossRef]
114. Rodríguez-Otamendi, D.I.; Meza-Laguna, V.; Acosta, D.; Álvarez-Zauco, E.; Huerta, L.; Basiuk, V.A.; Basiuk, E.V. Eco-friendly synthesis of graphene oxidesilver nanoparticles hybrids: The effect of amine derivatization. *Diam. Relat. Mater.* **2021**, *111*, 108208. [CrossRef]
115. Menazea, A.; Ahmed, M. Synthesis and antibacterial activity of graphene oxide decorated by silver and copper oxide nanoparticles. *J. Mol. Struct.* **2020**, *1218*, 128536. [CrossRef]
116. Menazea, A.; Ahmed, M. Silver and copper oxide nanoparticles-decorated graphene oxide via pulsed laser ablation technique: Preparation, characterization, and photoactivated antibacterial activity. *Nano-Struct. Nano-Objects* **2020**, *22*, 100464. [CrossRef]
117. Chowdhuri, A.R.; Tripathy, S.; Chandra, S.; Roy, S.; Sahu, S.K. A ZnO decorated chitosan–graphene oxide nanocomposite shows significantly enhanced antimicrobial activity with ROS generation. *RSC Adv.* **2015**, *5*, 49420–49428. [CrossRef]
118. Qiu, J.; Liu, L.; Chen, B.; Qiao, Y.; Cao, H.; Zhu, H.; Liu, X. Graphene oxide as a dual Zn/Mg ion carrier and release platform: Enhanced osteogenic activity and antibacterial properties. *J. Mater. Chem. B* **2018**, *6*, 2004–2012. [CrossRef] [PubMed]
119. Padmavathy, N.; Vijayaraghavan, R. Enhanced bioactivity of ZnO nanoparticles—An antimicrobial study. *Sci. Technol. Adv. Mater.* **2008**, *9*, 035004. [CrossRef]
120. Lyu, H.; He, Z.; Chan, Y.K.; He, X.; Yu, Y.; Deng, Y. Hierarchical ZnO Nanotube/Graphene Oxide Nanostructures Endow Pure Zn Implant with Synergistic Bactericidal Activity and Osteogenicity. *Ind. Eng. Chem. Res.* **2019**, *58*, 19377–19385. [CrossRef]
121. Wang, Y.-W.; Cao, A.; Jiang, Y.; Zhang, X.; Liu, J.-H.; Liu, Y.; Wang, H. Superior antibacterial activity of zinc oxide/graphene oxide composites originating from high zinc concentration localized around bacteria. *ACS Appl. Mater. Interfaces* **2014**, *6*, 2791–2798. [CrossRef] [PubMed]
122. Vanithakumari, S.; Jena, G.; Sofia, S.; Thinaharan, C.; George, R.; Philip, J. Fabrication of superhydrophobic titanium surfaces with superior antibacterial properties using graphene oxide and silanized silica nanoparticles. *Surf. Coat. Technol.* **2020**, *400*, 126074. [CrossRef]
123. Li, X.; Zhao, Y.; Wu, W.; Chen, J.; Chu, G.; Zou, H. Synthesis and characterizations of graphene–copper nanocomposites and their antifriction application. *J. Ind. Eng. Chem.* **2014**, *20*, 2043–2049. [CrossRef]
124. Rubilar, O.; Rai, M.; Tortella, G.; Diez, M.C.; Seabra, A.B.; Durán, N. Biogenic nanoparticles: Copper, copper oxides, copper sulphides, complex copper nanostructures and their applications. *Biotechnol. Lett.* **2013**, *35*, 1365–1375. [CrossRef] [PubMed]
125. Zhang, K.; Suh, J.M.; Lee, T.H.; Cha, J.H.; Choi, J.-W.; Jang, H.W.; Varma, R.S.; Shokouhimehr, M. Copper oxide–graphene oxide nanocomposite: Efficient catalyst for hydrogenation of nitroaromatics in water. *Nano Converg.* **2019**, *6*, 6. [CrossRef] [PubMed]
126. Mishra, A. Study of organic pollutant removal capacity for magnetite@ graphene oxide nanocomposites. *Vacuum* **2018**, *157*, 524–529. [CrossRef]
127. Haseen, U.; Ahmad, H.; Umar, K.; Parveen, T. Application of magnetite–graphene oxide for wastewater treatment. In *Graphene-Based Nanotechnologies for Energy and Environmental Applications*; Elsevier: Amsterdam, The Netherlands, 2019; pp. 195–203. [CrossRef]
128. Mao, M.; Zhang, W.; Huang, Z.; Huang, J.; Wang, J.; Li, W.; Gu, S. Graphene Oxide-Copper Nanocomposites Suppress Cariogenic Streptococcus mutans Biofilm Formation. *Int. J. Nanomed.* **2021**, *16*, 7727–7739. [CrossRef] [PubMed]
129. Li, Y.; Wang, W.; Gong, H.; Xu, J.; Yu, Z.; Wei, Q.; Tang, D. Graphene-coated copper-doped ZnO quantum dots for sensitive photoelectrochemical bioanalysis of thrombin triggered by DNA nanoflowers. *J. Mater. Chem. B* **2021**, *9*, 6818–6824. [CrossRef] [PubMed]
130. Yakout, A.A.; Alshitari, W.; Akhdhar, A. Synergistic effect of Cu-nanoparticles and β-cyclodextrin functionalized reduced graphene oxide nanocomposite on the adsorptive remediation of tetracycline antibiotics. *Carbohydr. Polym.* **2021**, *273*, 118528. [CrossRef]
131. Xu, X.; Tan, R.; Lv, X.; Geng, C.; Li, Y.; Cui, B.; Fang, Y. Non-enzymatic electrochemical detection of glucose using Ni–Cu bimetallic alloy nanoparticles loaded on reduced graphene oxide through a one-step synthesis strategy. *Anal. Methods* **2021**, *13*, 5628–5637. [CrossRef] [PubMed]

132. Sharma, T.S.K.; Hwa, K.-Y. Rational design and preparation of copper vanadate anchored on sulfur doped reduced graphene oxide nanocomposite for electrochemical sensing of antiandrogen drug nilutamide using flexible electrodes. *J. Hazard. Mater.* **2021**, *410*, 124659. [CrossRef] [PubMed]
133. Gao, J.; Liu, H.; Wu, K.; Yan, J.; Tong, C. A novel nonenzymatic ascorbic acid electrochemical sensor based on gold nanoparticals-chicken egg white-copper phosphate-graphene oxide hybrid nanoflowers. *Nanotechnology* **2021**, *32*, 325504. [CrossRef]
134. Singh, P.; Mandal, S.; Roy, D.; Chanda, N. Facile Detection of Blood Creatinine Using Binary Copper–Iron Oxide and rGO-Based Nanocomposite on 3D Printed Ag-Electrode under POC Settings. *ACS Biomater. Sci. Eng.* **2021**, *7*, 3446–3458. [CrossRef]
135. Xu, F.; Qiao, Z.; Luo, L.; He, X.; Lei, Y.; Tang, J.; Shi, H.; Wang, K. A label-free cyclic amplification strategy for microRNA detection by coupling graphene oxide-controlled adsorption with superlong poly(thymine)-hosted fluorescent copper nanoparticles. *Talanta* **2022**, *243*, 123323. [CrossRef]
136. Huang, J.; He, J.; Xu, K.; Xiang, Y.; Luo, Y. Diclofenac degradation by activating peroxydisulfate via well-dispersed GO/Cu_2O nano-composite. *Environ. Sci. Pollut. Res.* **2022**, *29*, 41776–41787. [CrossRef] [PubMed]
137. Lou, G.; Chen, Y.; Xu, J.; Qian, Y.; Cheng, H.; Wei, Z.; Yang, Y.; Shen, L.; Shuai, C. Preparation of Graphene Oxide-loaded Nickel with Excellent Antibacterial Property by Magnetic Field-Assisted Scanning Jet Electrodeposition. *Int. J. Bioprint.* **2021**, *8*, 432. [CrossRef] [PubMed]
138. Niu, H.; Cai, S.; Liu, X.; Huang, X.; Chen, J.; Wang, S.; Zhang, S. A novel electrochemical sandwich-like immunosensor based on carboxyl $Ti_3C_2T_x$ MXene and rhodamine b/gold/reduced graphene oxide for *Listeria monocytogenes*. *Anal. Methods* **2022**, *14*, 843–849. [CrossRef] [PubMed]
139. Valencia-Llano, C.H.; Solano, M.A.; Grande-Tovar, C.D. Nanocomposites of Chitosan/Graphene Oxide/Titanium Dioxide Nanoparticles/Blackberry Waste Extract as Potential Bone Substitutes. *Polymers* **2021**, *13*, 3877. [CrossRef] [PubMed]
140. Tamilarasan, P.; Ramaprabhu, S. Integration of polymerized ionic liquid with graphene for enhanced CO_2 adsorption. *J. Mater. Chem. A* **2014**, *3*, 101–108. [CrossRef]
141. Kostoglou, N.; Constantinides, G.; Charalambopoulou, G.; Steriotis, T.; Polychronopoulou, K.; Li, Y.; Liao, K.; Ryzhkov, V.; Mitterer, C.; Rebholz, C. Nanoporous spongy graphene: Potential applications for hydrogen adsorption and selective gas separation. *Thin Solid Films* **2015**, *596*, 242–249. [CrossRef]
142. Zhao, Y.; Ding, H.; Zhong, Q. Synthesis and characterization of MOF-aminated graphite oxide composites for CO_2 capture. *Appl. Surf. Sci.* **2013**, *284*, 138–144. [CrossRef]
143. Li, P.; Zeng, H.C. Hierarchical Nanocomposite by the Integration of Reduced Graphene Oxide and Amorphous Carbon with Ultrafine MgO Nanocrystallites for Enhanced CO_2 Capture. *Environ. Sci. Technol.* **2017**, *51*, 12998–13007. [CrossRef] [PubMed]
144. Oh, J.; Mo, Y.-H.; Le, V.-D.; Lee, S.; Han, J.; Park, G.; Kim, Y.-H.; Park, S.-E.; Park, S. Borane-modified graphene-based materials as CO_2 adsorbents. *Carbon* **2014**, *79*, 450–456. [CrossRef]
145. Sui, Z.-Y.; Cui, Y.; Zhu, J.-H.; Han, B.-H. Preparation of Three-Dimensional Graphene Oxide–Polyethylenimine Porous Materials as Dye and Gas Adsorbents. *ACS Appl. Mater. Interfaces* **2013**, *5*, 9172–9179. [CrossRef]
146. Sui, Z.-Y.; Meng, Y.-N.; Xiao, P.-W.; Zhao, Z.-Q.; Wei, Z.-X.; Han, B.-H. Nitrogen-Doped Graphene Aerogels as Efficient Supercapacitor Electrodes and Gas Adsorbents. *ACS Appl. Mater. Interfaces* **2015**, *7*, 1431–1438. [CrossRef] [PubMed]
147. Chowdhury, S.; Balasubramanian, R. Highly efficient, rapid and selective CO_2 capture by thermally treated graphene nanosheets. *J. CO2 Util.* **2016**, *13*, 50–60. [CrossRef]
148. Li, W.; Yang, H.; Jiang, X.; Liu, Q. Highly selective CO_2 adsorption of ZnO based N-doped reduced graphene oxide porous nanomaterial. *Appl. Surf. Sci.* **2016**, *360*, 143–147. [CrossRef]
149. Huang, W.; Zhou, X.; Xia, Q.; Peng, J.; Wang, H.; Li, Z. Preparation and Adsorption Performance of GrO@Cu-BTC for Separation of CO_2/CH_4. *Ind. Eng. Chem. Res.* **2014**, *53*, 11176–11184. [CrossRef]
150. Liu, S.; Sun, L.; Xu, F.; Zhang, J.; Jiao, C.; Li, F.; Li, Z.; Wang, S.; Wang, Z.; Jiang, X.; et al. Nanosized Cu-MOFs induced by graphene oxide and enhanced gas storage capacity. *Energy Environ. Sci.* **2013**, *6*, 818–823. [CrossRef]
151. Ganesan, A.; Shaijumon, M.M. Activated graphene-derived porous carbon with exceptional gas adsorption properties. *Microporous Mesoporous Mater.* **2016**, *220*, 21–27. [CrossRef]
152. Meng, L.-Y.; Park, S.-J. Effect of exfoliation temperature on carbon dioxide capture of graphene nanoplates. *J. Colloid Interface Sci.* **2012**, *386*, 285–290. [CrossRef] [PubMed]
153. He, Y.; Wang, F. Hydrate-based CO_2 capture: Kinetic improvement *via* graphene-carried $-SO_3^-$ and Ag nanoparticles. *J. Mater. Chem. A* **2018**, *6*, 22619–22625. [CrossRef]
154. Chowdhury, S.; Parshetti, G.K.; Balasubramanian, R. Post-combustion CO_2 capture using mesoporous TiO_2/graphene oxide nanocomposites. *Chem. Eng. J.* **2015**, *263*, 374–384. [CrossRef]
155. Mishra, A.K.; Ramaprabhu, S. Enhanced CO_2 capture in Fe_3O_4-graphene nanocomposite by physicochemical adsorption. *J. Appl. Phys.* **2014**, *116*, 064306. [CrossRef]
156. Mishra, A.K.; Ramaprabhu, S. Nanostructured polyaniline decorated graphene sheets for reversible CO_2 capture. *J. Mater. Chem.* **2012**, *22*, 3708–3712. [CrossRef]
157. Witoon, T.; Numpilai, T.; Phongamwong, T.; Donphai, W.; Boonyuen, C.; Warakulwit, C.; Chareonpanich, M.; Limtrakul, J. Enhanced activity, selectivity and stability of a CuO-ZnO-ZrO_2 catalyst by adding graphene oxide for CO_2 hydrogenation to methanol. *Chem. Eng. J.* **2018**, *334*, 1781–1791. [CrossRef]

158. Wang, C.L.; Li, Y.; Liu, C.L. Sorption of uranium from aqueous solutions with graphene oxide. *J. Radioanal. Nucl. Chem. Artic.* **2015**, *304*, 1017–1025. [CrossRef]
159. Li, Y.; Wang, C.; Guo, Z.; Liu, C.; Wu, W. Sorption of thorium(IV) from aqueous solutions by graphene oxide. *J. Radioanal. Nucl. Chem.* **2014**, *299*, 1683–1691. [CrossRef]
160. Mondal, N.K.; Chakraborty, S. Adsorption of Cr(VI) from aqueous solution on graphene oxide (GO) prepared from graphite: Equilibrium, kinetic and thermodynamic studies. *Appl. Water Sci.* **2020**, *10*, 61. [CrossRef]
161. Lingamdinne, L.P.; Koduru, J.R.; Roh, H.; Choi, Y.-L.; Chang, Y.-Y.; Yang, J.-K. Adsorption removal of Co(II) from waste-water using graphene oxide. *Hydrometallurgy* **2016**, *165*, 90–96. [CrossRef]
162. Wang, H.; Yuan, X.; Wu, Y.; Huang, H.; Zeng, G.; Liu, Y.; Wang, X.; Lin, N.; Qi, Y. Adsorption characteristics and behaviors of graphene oxide for Zn(II) removal from aqueous solution. *Appl. Surf. Sci.* **2013**, *279*, 432–440. [CrossRef]
163. Yang, A.; Zhu, Y.; Huang, C.P. Facile preparation and adsorption performance of graphene oxide-manganese oxide composite for uranium. *Sci. Rep.* **2018**, *8*, 9058. [CrossRef]
164. Zhang, Z.-B.; Qiu, Y.-F.; Dai, Y.; Wang, P.-F.; Gao, B.; Dong, Z.-M.; Cao, X.-H.; Liu, Y.-H.; Le, Z.-G. Synthesis and application of sulfonated graphene oxide for the adsorption of uranium(VI) from aqueous solutions. *J. Radioanal. Nucl. Chem. Artic.* **2016**, *310*, 547–557. [CrossRef]
165. Chen, S.; Hong, J.; Yang, H.; Yang, J. Adsorption of uranium (VI) from aqueous solution using a novel graphene oxide-activated carbon felt composite. *J. Environ. Radioact.* **2013**, *126*, 253–258. [CrossRef] [PubMed]
166. Jiang, T.; Liu, W.; Mao, Y.; Zhang, L.; Cheng, J.; Gong, M.; Zhao, H.; Dai, L.; Zhang, S.; Zhao, Q. Adsorption behavior of copper ions from aqueous solution onto graphene oxide–CdS composite. *Chem. Eng. J.* **2014**, *259*, 603–610. [CrossRef]
167. Wu, S.; Zhang, K.; Wang, X.; Jia, Y.; Sun, B.; Luo, T.; Meng, F.; Jin, Z.; Lin, D.; Shen, W.; et al. Enhanced adsorption of cadmium ions by 3D sulfonated reduced graphene oxide. *Chem. Eng. J.* **2014**, *262*, 1292–1302. [CrossRef]
168. Bulin, C.; Ma, Z.; Guo, T.; Li, B.; Zhang, Y.; Zhang, B.; Xing, R.; Ge, X. Magnetic graphene oxide nanocomposite: One-pot preparation, adsorption performance and mechanism for aqueous Mn(II) and Zn(II). *J. Phys. Chem. Solids* **2021**, *156*, 110130. [CrossRef]
169. Alimohammady, M.; Jahangiri, M.; Kiani, F.; Tahermansouri, H. Correction: Highly efficient simultaneous adsorption of Cd(ii), Hg(ii) and As(iii) ions from aqueous solutions by modification of graphene oxide with 3-aminopyrazole: Central composite design optimization. *New J. Chem.* **2019**, *43*, 19437. [CrossRef]
170. Tan, L.; Wang, J.; Liu, Q.; Sun, Y.; Jing, X.; Liu, L.; Liu, J.; Song, D. The synthesis of a manganese dioxide–iron oxide–graphene magnetic nanocomposite for enhanced uranium(vi) removal. *New J. Chem.* **2014**, *39*, 868–876. [CrossRef]
171. Singh, S.; Anil, A.G.; Khasnabis, S.; Kumar, V.; Nath, B.; Adiga, V.; Naik, T.S.K.; Subramanian, S.; Kumar, V.; Singh, J.; et al. Sustainable removal of Cr(VI) using graphene oxide-zinc oxide nanohybrid: Adsorption kinetics, isotherms and thermodynamics. *Environ. Res.* **2021**, *203*, 111891. [CrossRef]
172. Wu, P.; Wang, Y.; Hu, X.; Yuan, D.; Liu, Y.; Liu, Z. Synthesis of magnetic graphene oxide nanoribbons composite for the removal of Th(IV) from aqueous solutions. *J. Radioanal. Nucl. Chem. Artic.* **2018**, *319*, 1111–1118. [CrossRef]
173. Bulin, C.; Zhang, Y.; Li, B.; Zhang, B. Removal performance of aqueous Co(II) by magnetic graphene oxide and adsorption mechanism. *J. Phys. Chem. Solids* **2020**, *144*, 109483. [CrossRef]
174. Guo, Y.; Deng, J.; Zhu, J.; Zhou, X.; Bai, R. Removal of mercury(ii) and methylene blue from a wastewater environment with magnetic graphene oxide: Adsorption kinetics, isotherms and mechanism. *RSC Adv.* **2016**, *6*, 82523–82536. [CrossRef]
175. Huang, D.; Li, B.; Wu, M.; Kuga, S. Graphene Oxide-Based Fe–Mg (Hydr)oxide Nanocomposite as Heavy Metals Adsorbent. *J. Chem. Eng. Data* **2018**, *63*, 2097–2105. [CrossRef]
176. Jun, B.-M.; Kim, S.; Kim, Y.; Her, N.; Heo, J.; Han, J.; Jang, M.; Park, C.M.; Yoon, Y. Comprehensive evaluation on removal of lead by graphene oxide and metal organic framework. *Chemosphere* **2019**, *231*, 82–92. [CrossRef] [PubMed]
177. Hu, B.; Hu, Q.; Li, X.; Pan, H.; Tang, X.; Chen, C.; Huang, C. Rapid and highly efficient removal of Eu(III) from aqueous solutions using graphene oxide. *J. Mol. Liq.* **2017**, *229*, 6–14. [CrossRef]
178. Chen, W.; Wang, L.; Zhuo, M.; Wang, Y.; Fu, S.; Li, Y.; Wu, S. Reusable colloidal graphene oxide suspensions combined with dialysis bags for recovery of trace Y(iii) from aqueous solutions. *RSC Adv.* **2014**, *4*, 58778–58787. [CrossRef]
179. Yan, L.; Zhao, Q.; Jiang, T.; Liu, X.; Li, Y.; Fang, W.; Yin, H. Adsorption characteristics and behavior of a graphene oxide–Al_{13} composite for cadmium ion removal from aqueous solutions. *RSC Adv.* **2015**, *5*, 67372–67379. [CrossRef]
180. Li, D.; Zhang, B.; Xuan, F. The sorption of Eu(III) from aqueous solutions by magnetic graphene oxides: A combined experimental and modeling studies. *J. Mol. Liq.* **2015**, *211*, 203–209. [CrossRef]
181. Kumar, S.; Nair, R.R.; Pillai, P.B.; Gupta, S.N.; Iyengar, M.A.R.; Sood, A.K. Graphene Oxide–$MnFe_2O_4$ Magnetic Nanohybrids for Efficient Removal of Lead and Arsenic from Water. *ACS Appl. Mater. Interfaces* **2014**, *6*, 17426–17436. [CrossRef]
182. Neolaka, Y.A.; Lawa, Y.; Naat, J.N.; Riwu, A.A.; Iqbal, M.; Darmokoesoemo, H.; Kusuma, H.S. The adsorption of Cr(VI) from water samples using graphene oxide-magnetic (GO-Fe_3O_4) synthesized from natural cellulose-based graphite (kusambi wood or Schleichera oleosa): Study of kinetics, isotherms and thermodynamics. *J. Mater. Res. Technol.* **2020**, *9*, 6544–6556. [CrossRef]
183. Tan, L.; Liu, Q.; Song, D.; Jing, X.; Liu, J.; Li, R.; Hu, S.; Liu, L.; Wang, J. Uranium extraction using a magnetic $CoFe_2O_4$–graphene nanocomposite: Kinetics and thermodynamics studies. *New J. Chem.* **2015**, *39*, 2832–2838. [CrossRef]
184. Shao, L.; Wang, X.; Ren, Y.; Wang, S.; Zhong, J.; Chu, M.; Tang, H.; Luo, L.; Xie, D. Facile fabrication of magnetic cucurbit[6]uril/graphene oxide composite and application for uranium removal. *Chem. Eng. J.* **2016**, *286*, 311–319. [CrossRef]

185. Song, X.; Tan, L.; Sun, X.; Ma, H.; Zhu, L.; Yi, X.; Dong, Q.; Gao, J. Facile preparation of $NiCo_2O_4$@rGO composites for the removal of uranium ions from aqueous solutions. *Dalton Trans.* **2016**, *45*, 16931–16937. [CrossRef] [PubMed]
186. El-Maghrabi, H.; Abdelmaged, S.M.; Nada, A.; Zahran, F.; El-Wahab, S.A.; Yahea, D.; Hussein, G.; Atrees, M. Magnetic graphene based nanocomposite for uranium scavenging. *J. Hazard. Mater.* **2016**, *322*, 370–379. [CrossRef] [PubMed]
187. Dai, Z.; Sun, Y.; Zhang, H.; Ding, D.; Li, L. Highly Efficient Removal of Uranium(VI) from Wastewater by Polyamidoxime/Polyethyleneimine Magnetic Graphene Oxide. *J. Chem. Eng. Data* **2019**, *64*, 5797–5805. [CrossRef]
188. Yang, A.; Zhu, Y.; Li, P.; Huang, C.P. Preparation of a magnetic reduced-graphene oxide/tea waste composite for high-efficiency sorption of uranium. *Sci. Rep.* **2019**, *9*, 6471. [CrossRef] [PubMed]
189. Zhang, Q.; Zhao, D.; Ding, Y.; Chen, Y.; Li, F.; Alsaedi, A.; Hayat, T.; Chen, C. Synthesis of Fe–Ni/graphene oxide composite and its highly efficient removal of uranium(VI) from aqueous solution. *J. Clean. Prod.* **2019**, *230*, 1305–1315. [CrossRef]
190. Zong, P.; Cao, D.; Cheng, Y.; Wang, S.; Zhang, J.; Guo, Z.; Hayat, T.; Alharbi, N.S.; He, C. Carboxymethyl cellulose supported magnetic graphene oxide composites by plasma induced technique and their highly efficient removal of uranium ions. *Cellulose* **2019**, *26*, 4039–4060. [CrossRef]
191. Yang, A.; Wang, Z.; Zhu, Y. Facile preparation and highly efficient sorption of magnetic composite graphene oxide/Fe_3O_4/GC for uranium removal. *Sci. Rep.* **2021**, *11*, 8440. [CrossRef]
192. Lu, W.; Li, L.; Ding, D.; Dai, Z.; Tang, S.; Cao, C.; Liu, L.; Chen, D.T. Selective Adsorption of Uranium (VI) by Calix[6]arene-Modified Magnetic Graphene Oxide. *J. Nanosci. Nanotechnol.* **2018**, *18*, 8160–8168. [CrossRef] [PubMed]
193. Li, K.; Xiong, T.; Liao, J.; Lei, Y.; Zhang, Y.; Zhu, W. Design of MXene/graphene oxide nanocomposites with micro-wrinkle structure for efficient separating of uranium(VI) from wastewater. *Chem. Eng. J.* **2022**, *433*, 134449. [CrossRef]
194. Bi, C.; Zhang, C.; Ma, F.; Zhang, X.; Yang, M.; Nian, J.; Liu, L.; Dong, H.; Zhu, L.; Wang, Q.; et al. Growth of a mesoporous Zr-MOF on functionalized graphene oxide as an efficient adsorbent for recovering uranium (VI) from wastewater. *Microporous Mesoporous Mater.* **2021**, *323*, 111223. [CrossRef]
195. Liu, N.; Liang, H.; Tian, W.; Li, C.; Gao, Q.; Wang, N.; Guo, R.; Mo, Z. An antibacterial and antifouling amidoxime-functionalized graphene oxide aerogel for selective uranium adsorption in Salt Lake water. *Colloids Surf. A Physicochem. Eng. Asp.* **2022**, *649*, 129367. [CrossRef]
196. Xu, J.; Zhang, B.; Lu, Y.; Wang, L.; Tao, W.; Teng, X.; Ning, W.; Zhang, Z. Adsorption desulfurization performance of PdO/SiO_2@graphene oxide hybrid aerogel: Influence of graphene oxide. *J. Hazard. Mater.* **2021**, *421*, 126680. [CrossRef]
197. Oliveira, F.M.; Luxa, J.; Bouša, D.; Sofer, Z.; Gusmão, R. Electromagnetic Interference Shielding by Reduced Graphene Oxide Foils. *ACS Appl. Nano Mater.* **2022**, *5*, 6792–6800. [CrossRef]
198. Wang, Z.; Mao, B.; Wang, Q.; Yu, J.; Dai, J.; Song, R.; Pu, Z.; He, D.; Wu, Z.; Mu, S. Ultrahigh Conductive Copper/Large Flake Size Graphene Heterostructure Thin-Film with Remarkable Electromagnetic Interference Shielding Effectiveness. *Small* **2018**, *14*, e1704332. [CrossRef] [PubMed]
199. Pavlou, C.; Carbone, M.G.P.; Manikas, A.C.; Trakakis, G.; Koral, C.; Papari, G.; Andreone, A.; Galiotis, C. Effective EMI shielding behaviour of thin graphene/PMMA nanolaminates in the THz range. *Nat. Commun.* **2021**, *12*, 4655. [CrossRef] [PubMed]
200. Govindasamy, T.; Nandhakumar, M.; Mathew, N.K.; Kulangara, R.V.; Asapu, V.K.; Padmanapan, S.; Thangaian, D.T.; Subramanian, B. Electromagnetic shielding performance of reduced graphene oxide reinforced iron oxide nanostructured materials prepared by polyol method. *J. Mater. Res.* **2022**, *37*, 1216–1230. [CrossRef]
201. Singh, A.K.; Kumar, A.; Srivastava, A.; Yadav, A.N.; Haldar, K.; Gupta, V.; Singh, K. Lightweight reduced graphene oxide-ZnO nanocomposite for enhanced dielectric loss and excellent electromagnetic interference shielding. *Compos. Part B Eng.* **2019**, *172*, 234–242. [CrossRef]
202. Verma, M.; Singh, A.P.; Sambyal, P.; Singh, B.P.; Dhawan, S.K.; Choudhary, V. Barium ferrite decorated reduced graphene oxide nanocomposite for effective electromagnetic interference shielding. *Phys. Chem. Chem. Phys.* **2014**, *17*, 1610–1618. [CrossRef] [PubMed]
203. Shen, B.; Zhai, W.; Zheng, W. Ultrathin Flexible Graphene Film: An Excellent Thermal Conducting Material with Efficient EMI Shielding. *Adv. Funct. Mater.* **2014**, *24*, 4542–4548. [CrossRef]
204. Xiang, C.; Guo, R.; Lin, S.; Jiang, S.; Lan, J.; Wang, C.; Cui, C.; Xiao, H.; Zhang, Y. Lightweight and ultrathin TiO_2-Ti_3C_2TX/graphene film with electromagnetic interference shielding. *Chem. Eng. J.* **2018**, *360*, 1158–1166. [CrossRef]
205. Song, P.; Liang, C.; Wang, L.; Qiu, H.; Gu, H.; Kong, J.; Gu, J. Obviously improved electromagnetic interference shielding performances for epoxy composites via constructing honeycomb structural reduced graphene oxide. *Compos. Sci. Technol.* **2019**, *181*, 107698. [CrossRef]
206. Yang, X.; Fan, S.; Li, Y.; Guo, Y.; Li, Y.; Ruan, K.; Zhang, S.; Zhang, J.; Kong, J.; Gu, J. Synchronously improved electromagnetic interference shielding and thermal conductivity for epoxy nanocomposites by constructing 3D copper nanowires/thermally annealed graphene aerogel framework. *Compos. Part A Appl. Sci. Manuf.* **2019**, *128*, 105670. [CrossRef]
207. Jia, H.; Yang, X.; Kong, Q.-Q.; Xie, L.-J.; Guo, Q.-G.; Song, G.; Liang, L.-L.; Chen, J.-P.; Li, Y.; Chen, C.-M. Free-standing, anti-corrosion, super flexible graphene oxide/silver nanowire thin films for ultra-wideband electromagnetic interference shielding. *J. Mater. Chem. A* **2020**, *9*, 1180–1191. [CrossRef]
208. Li, D.-S.; Wang, S.-J.; Zhou, Y.; Jiang, L. Lightweight and hydrophobic Ni/GO/PVA composite aerogels for ultrahigh performance electromagnetic interference shielding. *Nanotechnol. Rev.* **2022**, *11*, 1722–1732. [CrossRef]

209. Zeng, Z.; Zhang, Y.; Ma, X.Y.D.; Shahabadi, S.I.S.; Che, B.; Wang, P.; Lu, X. Biomass-based honeycomb-like architectures for preparation of robust carbon foams with high electromagnetic interference shielding performance. *Carbon* **2018**, *140*, 227–236. [CrossRef]
210. Shen, Y.; Lin, Z.; Wei, J.; Xu, Y.; Wan, Y.; Zhao, T.; Zeng, X.; Hu, Y.; Sun, R. Facile synthesis of ultra-lightweight silver/reduced graphene oxide (rGO) coated carbonized-melamine foams with high electromagnetic interference shielding effectiveness and high absorption coefficient. *Carbon* **2021**, *186*, 9–18. [CrossRef]
211. Liu, X.; Wu, W.; Guo, B.; Cui, M.; Ma, H.; Zhang, Z.; Zhang, R. Facile fabrication of ultrathin graphene film with ultrahigh electrical conductivity and superb electromagnetic interference shielding effectiveness. *J. Mater. Chem. C* **2020**, *9*, 214–222. [CrossRef]
212. Abdel-Wahed, M.S.; El-Kalliny, A.S.; Badawy, M.I.; Attia, M.S.; Gad-Allah, T.A. Core double-shell $MnFe_2O_4$@rGO@TiO_2 superparamagnetic photocatalyst for wastewater treatment under solar light. *Chem. Eng. J.* **2019**, *382*, 122936. [CrossRef]
213. Adel, M.; Ahmed, M.A.; Mohamed, A.A. Synthesis and characterization of magnetically separable and recyclable crumbled $MgFe_2O_4$/reduced graphene oxide nanoparticles for removal of methylene blue dye from aqueous solutions. *J. Phys. Chem. Solids* **2020**, *149*, 109760. [CrossRef]
214. Sahoo, S.K.; Padhiari, S.; Biswal, S.; Panda, B.; Hota, G. Fe_3O_4 nanoparticles functionalized GO/g-C_3N_4 nanocomposite: An efficient magnetic nanoadsorbent for adsorptive removal of organic pollutants. *Mater. Chem. Phys.* **2020**, *244*, 122710. [CrossRef]
215. Li, D.; Hua, T.; Yuan, J.; Xu, F. Methylene blue adsorption from an aqueous solution by a magnetic graphene oxide/humic acid composite. *Colloids Surf. A Physicochem. Eng. Asp.* **2021**, *627*, 127171. [CrossRef]
216. De Farias, L.M.; Ghislandi, M.G.; de Aguiar, M.F.; Silva, D.B.; Leal, A.N.; Silva, F.d.A.; Fraga, T.J.; de Melo, C.P.; Alves, K.G. Electrospun polystyrene/graphene oxide fibers applied to the remediation of dye wastewater. *Mater. Chem. Phys.* **2021**, *276*, 125356. [CrossRef]
217. Cui, L.; Guo, X.; Wei, Q.; Wang, Y.; Gao, L.; Yan, L.; Yan, T.; Du, B. Removal of mercury and methylene blue from aqueous solution by xanthate functionalized magnetic graphene oxide: Sorption kinetic and uptake mechanism. *J. Colloid Interface Sci.* **2015**, *439*, 112–120. [CrossRef] [PubMed]
218. Bayantong, A.R.B.; Shih, Y.-J.; Ong, D.C.; Abarca, R.R.M.; Dong, C.-D.; de Luna, M.D.G. Adsorptive removal of dye in wastewater by metal ferrite-enabled graphene oxide nanocomposites. *Chemosphere* **2020**, *274*, 129518. [CrossRef]
219. Zhu, W.; Jiang, X.; Jiang, K.; Liu, F.; You, F.; Yao, C. Fabrication of Reusable Carboxymethyl Cellulose/Graphene Oxide Composite Aerogel with Large Surface Area for Adsorption of Methylene Blue. *Nanomaterials* **2021**, *11*, 1609. [CrossRef] [PubMed]
220. Verma, M.; Tyagi, I.; Kumar, V.; Goel, S.; Vaya, D.; Kim, H. Fabrication of GO–MnO2 nanocomposite using hydrothermal process for cationic and anionic dyes adsorption: Kinetics, isotherm, and reusability. *J. Environ. Chem. Eng.* **2021**, *9*, 106045. [CrossRef]
221. Ajeel, S.J.; Beddai, A.A.; Almohaisen, A.M.N. Preparation of alginate/graphene oxide composite for methylene blue removal. *Mater. Today Proc.* **2021**, *51*, 289–297. [CrossRef]
222. Bhattacharyya, A.; Ghorai, S.; Rana, D.; Roy, I.; Sarkar, G.; Saha, N.R.; Orasugh, J.T.; De, S.; Sadhukhan, S.; Chattopadhyay, D. Design of an efficient and selective adsorbent of cationic dye through activated carbon—Graphene oxide nanocomposite: Study on mechanism and synergy. *Mater. Chem. Phys.* **2020**, *260*, 124090. [CrossRef]
223. Du, R.; Cao, H.; Wang, G.; Dou, K.; Tsidaeva, N.; Wang, W. PVP modified rGO/$CoFe_2O_4$ magnetic adsorbents with a unique sandwich structure and superior adsorption performance for anionic and cationic dyes. *Sep. Purif. Technol.* **2022**, *286*, 120484. [CrossRef]
224. Al-Wasidi, A.S.; Abouelreash, Y.G.; AlReshaidan, S.; Naglah, A.M. Application of Novel Modified Chitosan Hydrogel Composite for the Efficient Removal of Eriochrome Black T and Methylene Blue Dyes from Aqueous Media. *J. Inorg. Organomet. Polym. Mater.* **2022**, *32*, 1142–1158. [CrossRef]
225. Cui, L.; Wang, Y.; Hu, L.; Gao, L.; Du, B.; Wei, Q. Mechanism of Pb(ii) and methylene blue adsorption onto magnetic carbonate hydroxyapatite/graphene oxide. *RSC Adv.* **2015**, *5*, 9759–9770. [CrossRef]
226. Kiranakumar, H.V.; Thejas, R.; Naveen, C.S.; Khan, M.I.; Prasanna, G.D.; Reddy, S.; Oreijah, M.; Guedri, K.; Bafakeeh, O.T.; Jameel, M. A review on electrical and gas-sensing properties of reduced graphene oxide-metal oxide nanocomposites. *Biomass Convers. Biorefin.* **2022**, 1–11. [CrossRef]
227. Majhi, S.M.; Mirzaei, A.; Kim, H.W.; Kim, S.S. Reduced Graphene Oxide (rGO)-Loaded Metal-Oxide Nanofiber Gas Sensors: An Overview. *Sensors* **2021**, *21*, 1352. [CrossRef] [PubMed]
228. Feng, Z.; Xu, Y.; Yue, W.; Adolfsson, K.H.; Wu, M. Recent progress in the use of graphene/po lymer composites to remove oil contaminants from water. *New Carbon Mater.* **2021**, *36*, 235–252. [CrossRef]